

The provenance of fertile off-craton lithospheric mantle: Sr–Nd isotope and chemical composition of garnet and spinel peridotite xenoliths from Vitim, Siberia

Dmitri A. Ionov^{a,b,c,*}, Igor Ashchepkov^d, Emil Jagoutz^c

^a*Abteilung Geochemie, Max-Planck-Institut für Chemie, Postfach 3060, D-55020 Mainz, Germany*

^b*Laboratoire de Tectonophysique (UMR 5568 CNRS), ISTEEM, Université Montpellier 2 case 049, 34095, Montpellier cedex 05, France*

^c*Abteilung Kosmochemie, Max-Planck Institut für Chemie, Postfach 3060, D-55020 Mainz, Germany*

^d*Institute of Geology, SB RAS, Koptyuga ave. 3, Novosibirsk 630090, Russia*

Received 26 July 2004; received in revised form 5 November 2004; accepted 1 December 2004

Abstract

Nd and Sr isotope compositions were obtained for pure garnet and pyroxene separates from coarse peridotite xenoliths from the Vitim volcanic province east of Lake Baikal. Internal Sm–Nd isochrons give ages of 24–42 Ma. These dates are older than the eruption age for the host picrite tuff (~16 Ma) indicating that garnet and clinopyroxene may not have been in isotopic equilibrium in the mantle (at 19–23 kbar, 990–1070 °C). In spite of their fertile major element chemistry, many peridotites have extremely depleted Nd and Sr isotope compositions (calculated from mineral analyses: $\epsilon_{\text{Nd}_t} = +14$ to $+27$; $^{87}\text{Sr}/^{86}\text{Sr} = 0.7017$ – 0.7028) and therefore plot outside the MORB field in the Sr–Nd isotope diagram. Sm–Nd and Rb–Sr model ages for unmetasomatised peridotites are concordant for each sample within ± 0.4 Ga and suggest a depletion event of a primitive mantle ~2 Gy ago, also consistent with Re–Os data on the same xenolith suite [Pearson, D.G., Irvine, G.J., Ionov, D.A., Boyd, F.R., Dreibus, G.E., 2004. Re–Os isotope systematics and Platinum Group Element fractionation during mantle melt extraction: a study of peridotite xenoliths from N. Lesotho and S. Namibian kimberlites, the Vitim volcanic field and massif peridotites from Beni Bousera. *Chem. Geol.* 208, 29–59]. This suggests that the mantle depletion event was roughly matched with formation of the mature continental crust in the region (~2.0 Ga according to U–Pb and Sm–Nd dating) and implies that the mantle peridotites have been attached to the continental lithosphere since that time and survived several major tectono-thermal events. The Paleoproterozoic formation age for the fairly fertile Vitim mantle domain indicates that average lithospheric mantle compositions cannot be used to assess lithospheric formation ages in continental off-craton mantle.

© 2004 Elsevier B.V. All rights reserved.

Keywords: Upper mantle; Garnet peridotite; Major elements; Trace elements; Sr–Nd isotopes; Lithospheric age

* Corresponding author. Present address: MPI für Chemie, Postfach 3060, D-55020 Mainz, Germany. Tel.: +49 6131 305 361; fax: +49 6131 371 051.

E-mail address: ionov@mpch-mainz.mpg.de (D.A. Ionov).

1. Introduction

Garnet-bearing peridotites are rare among xenoliths in off-craton alkali basaltic magmas, which normally only carry fragments of the shallow spinel facies lithospheric mantle. As a result, geochemical data on the garnet facies lithospheric mantle beyond cratons remain scarce and fragmentary. Garnet-bearing peridotite xenoliths discovered some 20 years ago in Miocene pyroclastic rocks on the Vitim plateau in Siberia (Fig. 1) (Ashchepkov et al., 1989) remain an important source of information about the most voluminous part of the continental lithospheric mantle (CLM) (Pearson et al., 2003).

The Vitim peridotite series is dominated by lherzolites with high modal clinopyroxene and garnet and is one of the most fertile, well-characterised mantle xenolith suites worldwide, in sharp contrast with highly refractory mantle underneath the nearby Siberian craton (Ionov, 2002; Ionov et al., 1993). The majority of the Vitim peridotites appear to have

experienced only small degrees of partial melting; many of them may be similar in modal and major element composition to model primitive mantle (Palme and O'Neill, 2003) or fertile asthenospheric mantle.

Another remarkable aspect of xenoliths from the Vitim Miocene tuff is their generally low degrees of post-melting metasomatism, in spite of the presence of rare discrete pyroxenites and veined peridotites (Ionov and Hofmann, 1995; Litasov et al., 2000). That inference was initially based on a small number of instrumental neutron activation analyses of pure minerals (Ionov et al., 1993) and preliminary results of an Sr–Nd isotope study published in Russian (Ionov and Jagoutz, 1988) and translated into English with an astonishing number of errors (Ionov and Jagoutz, 1989). While some new chemical data were reported recently (Ionov, 2004), trace element and isotope signatures of Vitim peridotites remain poorly characterised.

This paper reports Sr–Nd isotope and high-quality trace element data on minerals from some 20 xenoliths representing all major types of peridotites in the Vitim Miocene tuff suite. These geochemical data, together with Re–Os isotope analyses of many of those samples published recently by Pearson et al. (2004), shed new light on the origin and evolution of the lithospheric mantle beneath southern Siberia and other off-craton domains worldwide, in particular regarding fertile lithospheric mantle. Another objective of this study is to further investigate the residence of parent–daughter element pairs for the Sm–Nd and Rb–Sr isotope systems in spinel and garnet peridotites, which is relevant to interpretation of the isotope data. Furthermore, we present new, high-quality major element analyses and modal estimates for the whole-rock Vitim xenoliths. The data are used to better establish the partial melting conditions, explore possible links between chemical and isotope compositions of the rocks and better characterize modal, chemical and isotope heterogeneities in the CLM. We show that the lithospheric mantle beneath Vitim has largely preserved the chemical and isotopic signatures of ancient melting events (which is rare for mantle peridotites, e.g., Pearson and Nowell, 2002) and that the isotope data indicate the formation of the lithospheric mantle in the Paleoproterozoic, most likely ~2 Gy ago.

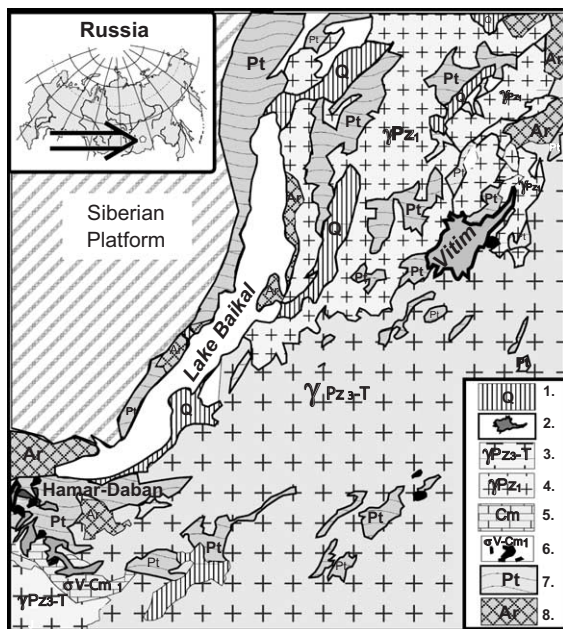


Fig. 1. Location of the Vitim volcanic field and a simplified geological map of the Trans-Baikal region (modified after Nalivkin, 1965): 1) Late Cenozoic sedimentary basins; 2) Cenozoic lava fields; 3–4) Phanerozoic granitoids; 5–6) Early Paleozoic ophiolite belts; 7–8) Paleoproterozoic to Archean metamorphic and igneous rocks.

2. Geological setting and samples

The Vitim plateau (or highland; elevations of 1000–1200 m) is located some 200–250 km east of central and northern Lake Baikal, in the region referred to in Russian as Zabaikalie (Trans-Baikal) (Fig. 1). An area about 100 km across in the central plateau, limited on three sides by a broad curve in the upper Vitim river, is covered with Cenozoic basaltic lava flows, with eroded remains of several eruption centres. The most common exposed basement rocks are Paleozoic to Early Mesozoic granitoids, which are commonly grouped together as the Angara–Vitim batholith (possibly one of the largest in the world). The granitoids enclose small blocks of Precambrian igneous and metamorphic rocks and Vendian–Cambrian volcanic–sedimentary sequences. The Precambrian rocks do not crop out in the area of the Cenozoic volcanism but occur elsewhere in the Trans-Baikal region (Fig. 1), indicating possible existence of ancient lithosphere before the Early Caledonian orogeny and related widespread intrusions of granitic magmas (Delvaux et al., 1995; Salnikova et al., 2001).

The Vitim plateau is clearly distinct, in terms of its relief, recent tectonic history, seismic activity (Sherman et al., 2004), gravity field etc. from the large-scale system of faults, grabens and mountain ranges that makes up the Baikal Rift Zone (BRZ) to the west (e.g., Petit et al., 2002). Nevertheless, it has been referred to by many authors, together with several other areas of basaltic volcanism south of the Siberian platform, as part of the BRZ (Glaser et al., 1999; Johnson et al., in press; Litasov et al., 2000; Rasskazov, 1994). One of the reasons for that is a widespread view that the whole rift zone (as well as a broad region around) is underlain by a large-scale “asthenospheric bulge”, which eroded much of the lithospheric mantle in a wide area beyond the central rift depressions. By contrast, recent tectonic and geophysical work (Petit et al., 1998), as well as re-assessment of the earlier data (Ionov, 2002), has found no evidence for the large-scale lithospheric thinning in central and northern BRZ nearest to the Vitim plateau. Many new geophysical and tectonic studies lend support to passive rifting due to far-field forces, which did not significantly affect the lithospheric mantle far away from the rift axis. Therefore, it is

appropriate to consider the Vitim volcanic field as part of the broad diffuse area of Cenozoic basaltic volcanism between the Siberian and North China cratons, i.e. not directly related to the opening and development of the Baikal rift.

The xenoliths for this study come from a picrite tuff deposit in the eastern part of the plateau (Ashchepkov et al., 1989; Ionov et al., 1993), also referred to as “Bereya area” and “picrobasalt quarry” (Glaser et al., 1999; Litasov et al., 2000). Precise dating of the picrite tuff is problematic because of alteration and abundant xenolith material. K–Ar analyses of handpicked tuff groundmass have yielded Middle Miocene age estimates between 15 ± 2 and 18 ± 1 Ma (unpublished data of I. Ashchepkov and A. Travin, 1995) while Esin et al. (1995) reported a K–Ar age of 16.3 ± 1.1 Ma. Most other volcanic rocks in the area are much younger (≤ 8 Ma); some of them host spinel and garnet–spinel xenoliths as well. However, the xenoliths from these young volcanics are smaller and less abundant than in the older picrite tuff, with spinel peridotites much more abundant than garnet-bearing xenoliths (Ashchepkov, 1991).

3. Sample preparation and analytical methods

The xenoliths range in size from 6 to 25 cm in longest dimension. They were cut using a diamond saw; once the rims had been removed, their interiors were crushed either in a hand steel mortar or in a bench-top jaw crusher, carefully cleaned after each sample to avoid cross-contamination. Aliquots of the crushed samples were ground in agate mortars to produce whole-rock powders. Another aliquot was washed and sieved. Appropriate size fractions (normally, 0.3–0.7 mm) were separated magnetically to yield sub-fractions enriched in olivine, pyroxenes and garnet. Nearly pure garnet fractions were obtained using heavy liquids. Most of the separates were treated ultrasonically to break mineral intergrowths and to clean grain surfaces. Ultra-pure minerals for trace element and isotopic analyses were handpicked in alcohol using strong sideward illumination, and then leached in diluted HF and HNO₃ or HCl prior to dissolution to remove possible contamination from grain surfaces and cracks. Fresh-looking groundmass was handpicked from crushed

picrite tuff and leached in diluted HCl to remove alteration products that may have been overlooked during handpicking.

The contents of major and minor elements in whole-rock peridotites were determined by wavelength-dispersive X-ray fluorescence (XRF) spectrometry at the University of Mainz. The rock powders were first ignited for ≥ 3 h at 1000° to turn all FeO into Fe_2O_3 and expel water and CO_2 . Glass beads produced by fusing 0.8 g of ignited powders with 4.8 g of dried LiB_4O_7 (1:7 dilution) were analysed on a Philips PW1404 instrument using ultramafic and mafic reference rock samples as external standards. Reference samples JP-1 and UBN were analysed as unknowns to control accuracy. Full duplicate and replicate analyses done in the same sample series typically reproduced within $\pm 0.1\%$ of averages for Si and Mg, $\pm 0.7\%$ for Ti, Al, Cr, Fe, Mn, Ni, Ca and $\pm 5\%$ for Na. Overall, the data have an improved accuracy and precision compared to previous XRF analyses of the same samples (Ionov et al., 1993) judging from reproducibility of duplicates, analyses of reference materials as unknowns and less scatter on element co-variation plots.

Major element compositions of minerals were determined in polished thin sections and grain mounts by wavelength-dispersive electron probe micro-beam analysis (EPMA) at MPI für Chemie (Mainz). A JEOL-200 instrument was used with an 15 kV accelerating voltage and sample current of 12 nA; analysis spot was 1–2 microns. Standards were natural and synthetic minerals; matrix corrections were by the ZAF method. Minerals in several samples were re-analysed next to laser-ablation pits to provide most reliable internal standard (CaO) data for calculating trace element values. Modal compositions were calculated from the whole-rock and mineral major element data by mass balance using least-squares regression.

Trace elements in pyroxenes and garnet were determined in grain mounts using a Finnigan Element-2 magnetic sector inductively coupled plasma mass-spectrometer (ICPMS) coupled with an automated UP-213 Nd-YAG laser-ablation (LA) microprobe at MPI für Chemie in Mainz. The analyses were done in low resolution mode, with ^{43}Ca as internal standard, using NIST SRM 612 glass for external calibration (Pearce et al., 1997).

Helium was used as carrier gas and mixed with Ar downstream of the ablation cell. The laser was operated with 1 mJ/pulse energy at 10 Hz (energy density 7 j/cm^2), ablation pits were normally 120 microns in diameter. MPI-DING reference glasses (Jochum et al., 2000) were analysed in each run for quality control. Analyses of homogeneous minerals repeated in different sessions usually reproduced within 1–6% at ≥ 0.2 ppm and within 5–20% at ≥ 0.005 ppm. The method of signal integration used in this study enables us to discard spurious signal components related both to instrumental problems and ablation of enriched micro-inclusions in depleted matrix. For example, the abundances of highly incompatible elements (LREE, Nb, Ta, Th, U) determined in Vitim garnet and orthopyroxene in this study are generally lower than those obtained by LA-ICPMS in another laboratory (Ionov, 2004) and yield consistent, spike-free patterns.

Solution ICPMS analyses were done on a Fisons (VG-Elemental) PQ2+Turbo (PlasmaQuad II+) instrument at Montpellier using the method of Ionov et al. (1992b). Whole-rock powders (~100 mg) and acid-leached mineral separates (10–20 mg) were dissolved by HF-HClO_4 attack in screw-top Teflon beakers. Dried samples were taken up in HNO_3 and diluted to 1:1000 (in 2% HNO_3) shortly before the analysis. In and Bi were used as internal standards for drift correction. Several series of composite synthetic external standards that enable corrections for oxide interference were used for calibration. Chemical blanks and 2–3 international reference materials were run with each sample batch (Ionov et al., 1992b).

Sr and Nd isotope analyses were done at the Cosmochemistry Division of Max-Planck-Institut für Chemie in Mainz using established procedures (Jagoutz and Wänke, 1986). Abundances of Rb, Sr, K, Sm and Nd were determined by isotope dilution (ID) in aliquots of the same pure, leached mineral separates that were analysed for the isotopic ratios. The mineral separates were dissolved by HF-HClO_4 attack in screw-top Teflon beakers. Elements for isotopic analyses were isolated using Dowex WX 50 and HDEHP ion-exchangers. Blank contribution is ≤ 7 pg for Nd and ≤ 55 pg for Sr. Isotopic measurements were performed on a single collector mass-spectrometer (constructed by E.J.). $^{87}\text{Sr}/^{86}\text{Sr}$ were

normalised to $^{86}\text{Sr}/^{88}\text{Sr}=0.1194$; $^{143}\text{Nd}/^{144}\text{Nd}$ were normalised to $^{146}\text{Nd}/^{144}\text{Nd}=0.7219$. The errors reported in Table 6 are 2σ in-run statistics. At the time of this study, the Eimer and Ahmend and La

Jolla standards yielded $^{87}\text{Sr}/^{86}\text{Sr}=0.70802\pm 2$ and $^{143}\text{Nd}/^{144}\text{Nd}=0.511890\pm 4$ (2σ). No corrections for blank contribution or defined values of standards were used.

Table 1
List of samples, P – T data and modal compositions, and available analytical data

Sample number	P core	T		Modal composition (wt.%)					WR XRF	WR solution ICPMS	LA/soil ^a ICPMS	$^{143}\text{Nd}/^{144}\text{Nd}$	$^{87}\text{Sr}/^{86}\text{Sr}$	Re–Os isotope	
		Core	Rim	Ol	Opx	Cpx	Gar	Spl							
<i>Garnet peridotites</i>															
313-1	21.9	1016	1056	57.8	18.1	13.2	10.9		+	(2)	opx, cpx, gar	cpx, gar		cpx, gar	
313-2 ¹	21.6	1061	1097	57.8	21.8	13.8	6.6			(2)	opx, cpx, gar	cpx, gar		cpx	
313-3	21.2	993	1038	58.6	17.1	13.4	10.9		+	(2)	opx, cpx, gar	cpx, gar		cpx, gar	
313-5	20.9	1071	n.d.	59.4	18.5	12.8	9.3		+		opx, cpx, gar				
313-6	21.5	1063	n.d.	61.6	15.9	12.6	9.9		+	(2)	(1)	cpx		cpx, gar	+
313-7	22.3	1073	n.d.	57.4	25.6	13.1	3.9		+		opx, cpx, gar				
313-8	21.5	1034	/1101/	51.9	21.1	13.9	13.1		+	(2)	opx, cpx, gar	cpx, gar		cpx	+
313-54 ¹	22.5	1047	1098	59.4	14.6	13.9	12.1			+	opx, cpx, gar ^a	cpx, gar		cpx, gar	
313-102	22.9	1053	1143	49.9	23.0	13.6	13.5		+	(2)	(2)				+
313-104	22.0	1032	1128	53.9	19.7	14.2	12.2		+	(2)	(2)				+
313-105	21.3	1034	1126	63.0	16.8	11.9	8.3		+	+	ol, opx, cpx, gar ^a	cpx, gar		cpx, gar	+
313-106	21.7	1029	1051	62.6	15.9	12.9	8.6		+	(2)	(2)				
313-112	23.1	1041	1054	55.8	21.1	10.5	12.7		+	(2)	(2)				
313-240	21.4	1035	1145	62.4	17.6	11.2	8.8		+	(2)	(2)	cpx		cpx	+
313-241	22.8	1063	1138	59.8	18.0	11.3	10.9		+	(2)	(2)				
<i>Garnet–spinel peridotites</i>															
313-37	21.5	1026	/1099/	55.5	24.7	14.7	4.9	0.2	+	(2)	opx, cpx, gar	cpx, gar		cpx, gar	+
313-110	20.7	1009	1049	63.0	14.4	13.1	9.1	0.5	+	+	(1)	cpx, gar		cpx	+
314-74	19.7	1026	/1154/	61.1	26.6	8.8	2.8	0.7	+	+	(1)	cpx		cpx	+
314-230	18.4	1013	n.d.	61.5	20.1	16.2	1.5	0.7	+		opx, cpx, gar				+
314-580	21.4	1067	/1124/	64.9	16.5	11.0	7.2	0.4	+		(1)	cpx		cpx	+
<i>Spinel peridotites (SP-1)</i>															
314-56	/15/	889	869	51.0	29.9	16.6		2.5	+	+	ol, opx, cpx ^a	cpx		cpx	+
314-58	/15/	878	854	55.4	27.9	14.2		2.5	+	+	(1)	cpx		cpx	+
<i>Spinel peridotites (SP-2)</i>															
314-5	/18/	1033	n.d.	75.7	22.0	1.8		0.5	+	(2)	opx, cpx				
314-6 ¹	/18/	998	n.d.	70.4	22.8	5.7		1.1		(2)	opx, cpx	cpx		cpx	+
314-59	/18/	1027	1069	56.8	25.4	16.0		1.8	+	+	(1)/cpx ^a	cpx		cpx	+
<i>Composite and veined garnet peridotites</i>															
313-4 ¹	20.1	1014	n.d.	52.2	14.1	14.4	19.3			(2)		cpx, gar		cpx, gar	
313-103	20.6	1026	n.d.								(3)	cpx, am, phl		cpx, am, phl	
313-114	21.8	1079	n.d.								(3)	cpx, gar, am		cpx, gar, am	
<i>Host volcanic rock</i>															
87-1										+		+		+	

Ol, olivine; opx, orthopyroxene; cpx, clinopyroxene; gar, garnet; am, amphibole; phl, phlogopite. Equilibration pressures (P) are after Nickel and Green (1985); temperatures (T) are after Brey and Köhler (1990). Modal and trace element data, other than obtained in this study (+), are from Ionov et al. (2004) (1), Ionov (2004) (2) and Ionov and Hofmann (1995) (3). Re–Os data are in Pearson et al. (2004).

^a Soution ICPMS analyses of minerals.

4. Petrography and major element compositions

4.1. Rock types

A list of samples analysed in this study is given in Table 1 together with pressure (P), temperature (T) and modal estimates, information about analytical work done on each sample and sources of additional data. All the xenoliths are medium- to coarse-grained; their textures can be broadly defined as protogranular. Strongly deformed (sheared) rocks are extremely rare (Ashchepkov, 1991; Glaser et al., 1999) and have not been included in this study. Garnet lherzolite (Fig. 2) is the most common xenolith type in the Vitim Miocene tuff (Ashchepkov et al., 1989; Ionov, 2004; Ionov et al., 1993). These rocks contain 4–13 wt.% of garnet, 11–14% of clinopyroxene and no interstitial spinel. Garnet grains range in shape from equant (Fig. 3a) to highly irregular; the latter commonly have abundant rounded inclusions of olivine, pyroxenes and spinel (Fig. 3b). Garnet grains commonly have kelyphite at rims and inside cracks (Fig. 3b). Garnet normally has larger grain size than other minerals and in many xenoliths is unevenly distributed on a centimeter-scale (Fig. 2). Its grains usually occur in clusters 2–4 cm across while the remainder of the rock

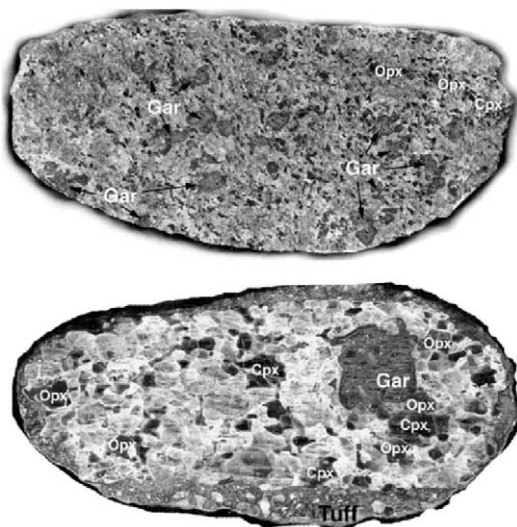
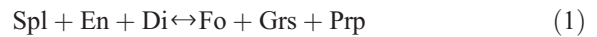


Fig. 2. Photographs of cut and polished garnet lherzolite xenoliths from the Vitim Miocene tuff. The horizontal size of the xenoliths is about 15 cm for the upper one and about 8 cm for the lower one. Large garnet grains and their clusters are irregularly distributed.

has little or no garnet (and no spinel; Fig. 2, top); in some xenoliths, large (1–2 cm) garnet grains are set in garnet-free matrix (Fig. 2, bottom).

Garnet–spinel peridotites differ from garnet peridotites primarily by the ubiquitous presence of interstitial spinel, which may be locally rimmed by garnet. The abundance of garnet varies broadly both within individual xenoliths on a centimeter-scale and between the xenoliths, from traces to ~10%. Textural relationships similar to those shown in Fig. 3b led Ionov et al. (1993) and Ionov (2004) to conclude that the garnets grew at the expense of spinel and pyroxenes (most likely owing to a decrease in temperature) as a result of the reaction:



Typical for garnet and garnet–spinel lherzolites is preferred linear orientation of large prismatic olivine grains (Fig. 3a and c). Some garnet-bearing xenoliths are composite or veined (Table 1). The size and abundance of garnet in xenolith 313-4 gradually increase from the centre to one side of that sample (Ionov, 2004) probably representing a transition zone from a normal garnet lherzolite to a garnet-rich segregation (without a sharp, cross-cutting contact between the two rock types).

Spinel peridotites are subdivided in two types. The first one (SP-1) has protogranular microstructure, with anhedral and unstrained minerals, no preferred mineral orientation and common spinel–pyroxene intergrowths. These rocks typically have high modal clinopyroxene and low equilibration temperatures (Table 1). The second type (SP-2) has subhedral, elongated olivine grains with slight to moderate preferred orientation (Kern et al., 1996). The appearance of those rocks in thin sections (Fig. 3c) is similar to that of garnet-free domains in the garnet–spinel peridotites.

Accessory amphibole and phlogopite are not common in the Vitim peridotites, rare phlogopite grains were found only in two xenoliths from this study: 314-56 (SP-1) and 313-110 (garnet–spinel). On the other hand, amphibole and phlogopite are common in pyroxenite xenoliths and pyroxene-rich veins in garnet peridotites. The proportion of pyroxenites and veined peridotites in the xenolith population appears to be less than 5–10%. Minerals of two amphibole-rich, phlogopite-bearing veins (Table

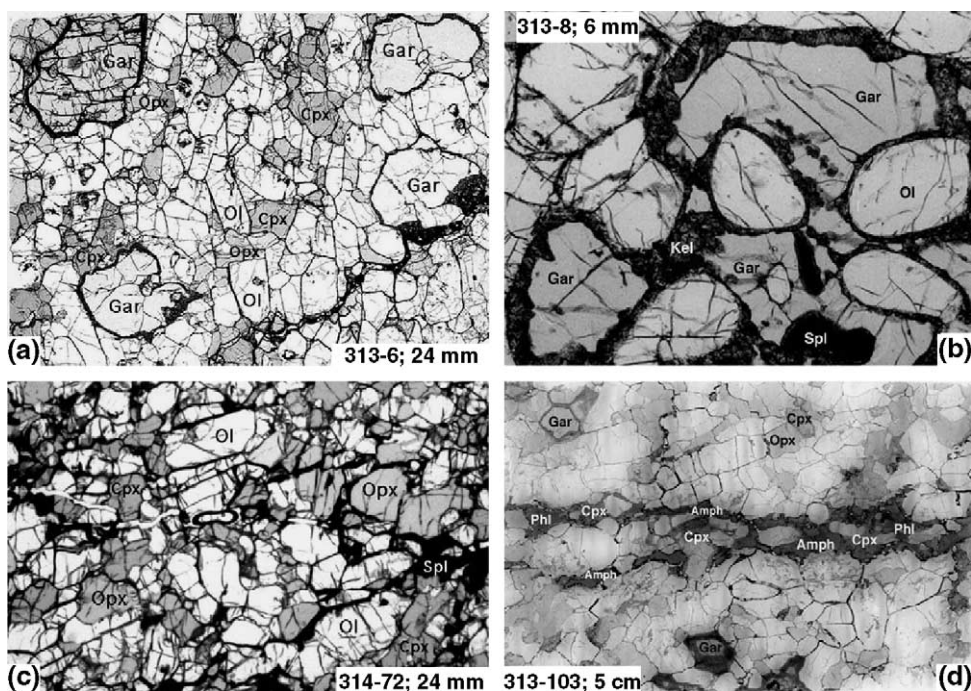


Fig. 3. (a–d) Photomicrographs of Vitim peridotite xenoliths in plane-polarized transmitted light. Sample numbers and the field of view along the long axis are indicated on each photograph. Ol, olivine; Opx, orthopyroxene; Cpx, clinopyroxene; Gar, garnet; Spl, spinel, Amph, amphibole, Phl, phlogopite, Kel, kelyphite. (a) Garnet lherzolite with large, equant, mainly inclusion-free and homogeneously distributed garnet grains; prismatic olivine grains with preferred linear orientation are common. Dark vein at bottom right is filled with host volcanic material and alteration products; these are locally present also at grain boundaries. (b) A large complex garnet grain with round to oval-shaped inclusions of mainly olivine and spinel. The garnet has fine-grained kelyphite aggregates (dark, cloudy) along rims and cracks. (c) High- T spinel lherzolite (SP-2 type) with preferred linear orientation of prismatic olivine. (d) Amph–Phl–Cpx vein in garnet lherzolite. Metasomatic clinopyroxene in the vein is grey to pale-green (in contrast to emerald-green Cpx in the host lherzolite). Garnet and orthopyroxene do not normally occur in direct contact with the metasomatic vein.

1; Ionov and Hofmann, 1995) were analysed for Sr–Nd isotopes. The veins have diffuse, poorly defined contacts. Vein 313-103 (Fig. 3d) represents a locally intermittent chain of coarse, mainly interstitial amphibole, phlogopite and metasomatic clinopyroxene. Vein 313-114 is mainly massive, anastomosing, 1–3 cm thick.

4.2. Whole-rock compositions

Major element compositions of Vitim peridotite xenoliths were earlier reported by Ionov et al. (1993) and Ionov (2004). Nearly all those samples were re-analysed in this study using ignited rock powders (Table 2). The change of mass on ignition ranges from -0.26% to $+0.35\%$ and thus demonstrates generally low degrees of alteration in the xenoliths. The mass

gain after ignition indicates that the oxidation of FeO to Fe_2O_3 (which can increase the mass up to 0.6% for fresh peridotites with $\Sigma\text{FeO}\sim 8\%$) is more significant than the loss of volatiles.

The new dataset from this study is more accurate and shows clear trends and less scatter on the MgO– Al_2O_3 (Fig. 4a), Mg–Si and other co-variation plots than the data from earlier work. The new analyses have similar MgO and FeO and slightly lower Al_2O_3 than those from Ionov et al. (1993) (recalculated to 100%) and plot mainly within the field of peridotites from Tariat, another well-studied central Asian xenolith locality (Fig. 4). Nevertheless, the new analyses confirm that the most fertile garnet lherzolites from Vitim typically have higher Al_2O_3 than spinel lherzolites from Tariat at similar MgO (Fig. 4a) and thus are slightly enriched in Al relative to

Table 2
XRF analyses of whole-rock Vitim xenoliths

Sample number	313-1	313-3	313-5	313-6	313-7	313-8	313-37	313-102	313-104	313-105	313-106	313-110	313-112	313-240	313-241
Rock	Gar lh	Gar lh	Gar lh	Gar lh	Gar lh	Gar lh	Gar–Spl	Gar lh	Gar lh	Gar lh	Gar lh	Gar–Spl	Gar lh	Gar lh	Gar lh
SiO ₂	45.03	44.83	44.61	44.87	45.82	45.37	45.73	45.53	45.19	44.55	44.35	44.20	45.26	44.41	44.64
TiO ₂	0.166	0.167	0.159	0.155	0.129	0.177	0.126	0.151	0.171	0.137	0.147	0.123	0.153	0.133	0.144
Al ₂ O ₃	4.14	3.85	3.73	3.73	2.74	4.58	2.99	4.76	4.43	3.23	3.42	3.52	4.28	3.35	3.84
Cr ₂ O ₃	0.390	0.396	0.389	0.386	0.331	0.408	0.398	0.411	0.373	0.360	0.400	0.403	0.385	0.367	0.387
FeO	8.12	8.28	8.28	8.41	7.80	7.94	7.99	8.16	8.11	8.12	8.29	8.19	8.20	8.29	8.23
MnO	0.14	0.13	0.13	0.13	0.12	0.14	0.12	0.15	0.14	0.13	0.13	0.13	0.14	0.13	0.13
NiO	0.251	0.259	0.260	0.254	0.263	0.238	0.259	0.232	0.242	0.262	0.267	0.266	0.250	0.261	0.255
MgO	38.64	38.51	38.93	39.18	39.34	37.51	38.64	37.05	37.70	40.37	39.46	39.60	38.62	40.17	39.24
CaO	2.96	3.29	2.95	2.95	2.82	3.53	3.29	3.43	3.49	2.87	3.05	3.06	2.84	2.76	2.88
Na ₂ O	0.28	0.29	0.32	0.27	0.31	0.28	0.31	0.33	0.34	0.28	0.30	0.28	0.24	0.26	0.25
K ₂ O	0.02	0.04	0.04	0.03	0.03	0.05	0.02	0.02	0.02	0.01	0.01	0.01	0.02	0.03	0.01
P ₂ O ₅	0.011	0.021	0.023	0.015	0.02	0.02	0.009	0.011	0.014	0.009	0.019	0.015	0.012	0.014	0.007
Sum	100.13	100.06	99.82	100.39	99.73	100.25	99.88	100.24	100.22	100.31	99.85	99.80	100.40	100.18	100.03
Mg#	0.895	0.892	0.893	0.893	0.900	0.894	0.896	0.890	0.892	0.899	0.895	0.896	0.894	0.896	0.895
C.M.I.	−0.12%	−0.11%	−0.26%	−0.17%	0.09%	−0.17%	−0.14%	0.08%	0.35%	0.32%	0.17%	−0.03%	0.23%	0.27%	0.24%

C.M.I., change of mass on ignition (≥ 3 h at 1000 °C). Positive values indicate overall weight gain due to oxidation of FeO to Fe₂O₃. 314-71a and 314-71b are full duplicates (two fused beads) of sample 314-71. JP-1 a and b are replicates of a JP-1 bead measured in two sessions together with the xenoliths. Data from Ionov et al. (1993) and Ionov (2004) for five samples which were not analyzed for major oxides in this study were used in the calculation of the average and median compositions.

Table 2 (continued)

Sample number	314-5	314-56	314-58	314-59	314-71a	314-71b	314-72	314-74	314-230	314-580	Average	Median	JP-1 (a)	JP-1 (b)	JP-1	UB-N
Rock	Spl lh	Spl lh	Spl lh	Spl lh	Spl lh	Spl lh	Spl lh	Gar–Spl	Gar–Spl	Gar–Spl	(29)	(29)	ignited	ignited	R.V.	ignited
SiO ₂	43.23	45.45	44.70	45.09	44.44	44.53	45.07	44.79	45.22	44.05	44.83	44.83	43.65	43.60	43.74	45.33
TiO ₂	0.076	0.182	0.141	0.121	0.164	0.163	0.116	0.091	0.152	0.169	0.15	0.15	0.017	0.011	0.00	0.120
Al ₂ O ₃	1.25	4.09	3.76	3.23	2.28	2.31	2.87	2.58	2.56	3.13	3.38	3.38	0.74	0.70	0.64	3.33
Cr ₂ O ₃	0.225	0.374	0.385	0.510	0.426	0.432	0.370	0.399	0.412	0.362	0.39	0.39	0.430	0.429	0.448	0.388
FeO	9.83	8.38	8.23	7.94	7.99	8.02	7.98	7.79	8.16	8.78	8.21	8.16	7.64	7.60	7.75	8.45
MnO	0.12	0.14	0.14	0.14	0.12	0.12	0.12	0.14	0.14	0.14	0.12	0.13	0.12	0.12	0.12	0.14
NiO	0.306	0.240	0.250	0.260	0.292	0.296	0.276	0.277	0.269	0.272	0.26	0.26	0.326	0.325	0.323	0.294
MgO	43.94	37.18	38.58	39.04	42.67	42.73	40.65	40.79	39.75	40.61	39.51	39.34	46.07	45.87	46.14	40.24
CaO	0.56	3.53	3.04	3.33	1.36	1.37	2.07	2.18	3.25	2.56	2.83	2.95	0.55	0.55	0.58	1.37
Na ₂ O	0.08	0.35	0.27	0.30	0.17	0.16	0.23	0.17	0.33	0.30	0.25	0.24	0.02	0.01	0.02	0.11
K ₂ O	0.01	0.02	0.02	0.01	0.03	0.03	0.03	0.03	0.04	0.03	0.03	0.02	0.00	0.01	0.00	0.02
P ₂ O ₅	0.015	0.010	0.010	0.010	0.010	0.011	0.018	0.010	0.017	0.013	0.01	0.01	0.00	0.00		0.01
Sum	99.64	99.96	99.53	99.99	99.96	100.18	99.81	99.25	100.31	100.43	99.97	99.95	99.56	99.22	99.77	99.81
Mg#	0.889	0.888	0.893	0.898	0.905	0.905	0.901	0.903	0.897	0.892	0.896	0.895	0.915	0.915	0.914	0.895
C.M.I.	0.09%	>0.0%	0.25%	0.17%	n.d.	n.d.	0.34%	0.06%	0.21%	0.25%			–2.43%			–12.2%

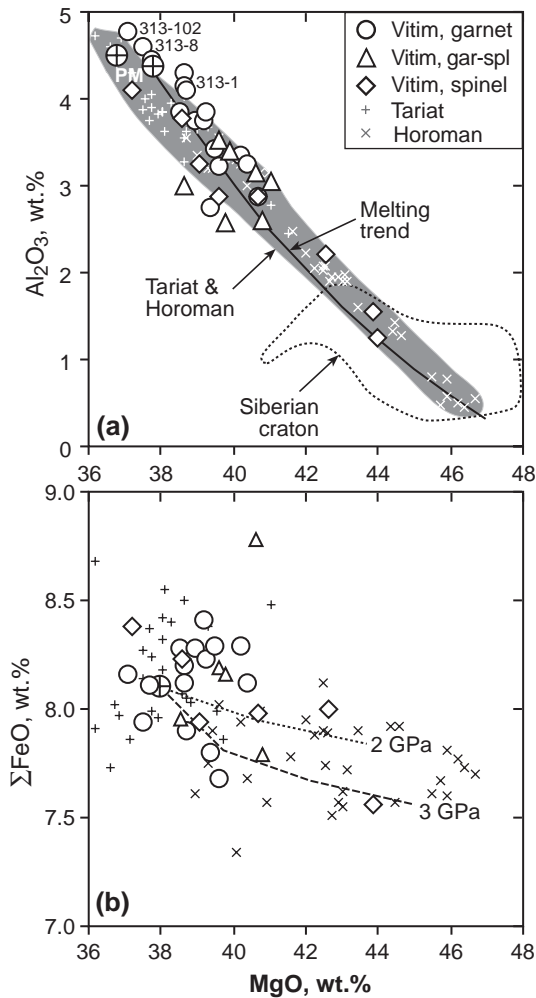


Fig. 4. Major-element co-variation plots for Vitim xenoliths. (a) MgO vs. Al_2O_3 . Al_2O_3 values for three samples from Ionov et al. (1993) were corrected for a systematic difference (6%) with analyses from this work. Also shown are calculated residues from polybaric (2.5–0.4 Ga) fractional melting of fertile spinel lherzolite (solid black line; Niu, 1997; Takazawa et al., 2000), and a combined field of peridotites from the Horoman massif, Japan (Takazawa et al., 2000) and peridotite xenoliths from Tariat, Mongolia (Press et al., 1986; unpublished data of D. Ionov, 2000, 2003). Major oxide compositions of these two peridotite suites are consistent with low (Tariat) to high (Horoman) degrees of shallow partial melting of a fertile protolith, and have not been significantly affected by metasomatism. Dashed line contours the field of peridotite xenoliths from the Udachnaya kimberlite on the Siberian craton ($\geq 90\%$ of samples from Boyd et al., 1997). PM, primitive mantle estimates after McDonough and Sun (1995) and Palme and O'Neill (2003). (b) MgO vs. FeO. Also shown are trends for partial melting residues at 2 and 3 GPa (Walter, 2003).

common fertile mantle (Ionov, 2004). By comparison, several garnet-poor and spinel Vitim peridotites have relatively low Al_2O_3 and plot below the combined Tariat–Horoman field on the Mg–Al diagram. As discussed by Ionov (2004), they may be products of post-melting “metamorphic differentiation”, complementary to the relatively Al-rich garnet lherzolites (Fig. 4a).

The majority of Vitim garnet peridotites are fertile rocks with high modal clinopyroxene and garnet and high contents of Al_2O_3 and CaO. Only about a quarter of xenoliths from this study contain $\leq 3\%$ Al_2O_3 , most of the latter are spinel (SP-2) and garnet–spinel peridotites. The generally fertile Vitim xenolith suite is distinct in terms of major element (Fig. 4a) and modal compositions from the typically refractory garnet and spinel peridotite xenoliths in kimberlites from the nearby Siberian craton (Fig. 1) (Ionov et al., 1993) and elsewhere (Pearson et al., 2003). In particular, the Vitim xenoliths overlap the fertile end of the “oceanic trend” of Boyd (1989) and have generally lower modal olivine and much lower Mg#Ol [$\text{Mg}/(\text{Mg}+\text{Fe})_{\text{at}}$ in olivine] than peridotite xenoliths from the Udachnaya kimberlite (Fig. 5).

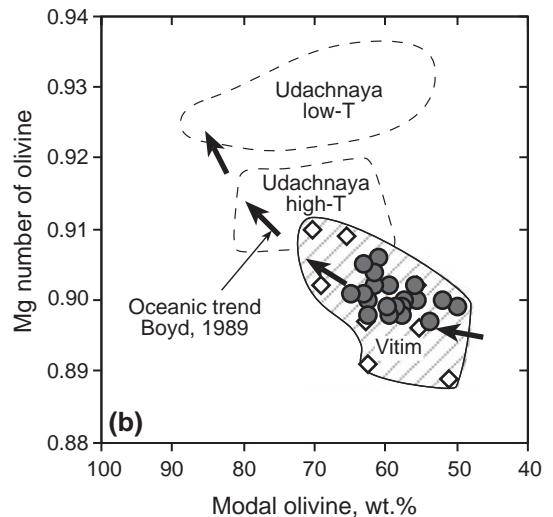


Fig. 5. Plot of modal olivine vs. Mg# in olivine (“Boyd diagram”). Also shown are fields for high-temperature and low-temperature peridotite xenoliths from the Udachnaya kimberlite (Boyd et al., 1997) and the “oceanic trend” after Boyd (1989).

4.3. Mineral major element compositions and P – T estimates

Major element compositions of minerals in representative garnet, garnet–spinel and spinel lherzolites from this study are given in Table 3. EPMA data for other Vitim xenoliths are given in electronic appendix in Ionov (2004). Mg#Ol in Vitim peridotites ranges from 0.885 to 0.91 (Fig. 5). Vitim garnets are low in chromium (0.9–1.4% Cr₂O₃ in cores and 1.0–1.6% in the rims) and calcium (4.8–5.2% CaO) and thus are distinct from much more Cr- and Ca-rich garnets in cratonic peridotites (Griffin et al., 1998; Pearson et al., 2003). Clinopyroxenes in fertile lherzolites have high Na₂O (1.6–2.15%) and Al₂O₃. Al contents in pyroxenes from garnet-bearing xenoliths tend to be lower than in pyroxenes from spinel lherzolites (Ionov et al., 1993). Pyroxenes from garnet, garnet–spinel and SP-2 peridotites typically have higher Al and Cr towards the rims; the contents of Ca increase towards the rims in orthopyroxene and decrease towards the rims in clinopyroxene.

Equilibration temperatures and pressures were estimated using EPMA data on cores of large mineral grains from a combination of the Ca–opx thermometer of Brey and Köhler (1990) and the barometer of Nickel and Green (1985). The garnet lherzolites equilibrated at 20.9–23.1 kbar and 993–1073 °C (Table 1; Fig. 6). This P – T range is more narrow than those reported earlier (Ionov, 2004; Ionov et al., 1993), possibly because of the use of more accurate average mineral compositions based on larger numbers of analyses for several samples. The new P – T estimates overlap the central part of the P – T trend calculated using the same method for garnet-bearing peridotites from Pali-Aike in Patagonia (one of few off-craton suites, for which a geotherm can be constructed from data on peridotites) (Fig. 6). The P – T estimates for garnet–spinel lherzolites range from 18.4 to 21.5 kbar and 1009 to 1065 °C. Some garnet–spinel rocks overlap the upper part of the P – T field defined by garnet lherzolites while others yield significantly lower pressures and hence come from shallower depths. Temperatures for SP-2 peridotites (1000–1030 °C) overlap the lower part of the T -range for the garnet-bearing xenoliths and are

much higher than for SP-1 peridotites (880–890 °C; Fig. 6).

Assuming that temperature gradually increases with depth, one can infer relative positions of the rock types in the lithospheric cross-section. The SP-1 rocks are from the shallow mantle above the spinel–garnet transition boundary for fertile peridotites. The SP-2 and garnet–spinel peridotites coexist in the depth range ~60–70 km (18–21 kbar). SP-2, garnet–spinel and garnet peridotites appear to be inter-layered in the depth range ~70–75 km (21–22 kbar). Garnet peridotites are dominant at greater depths. The main reason why garnet, garnet–spinel and spinel peridotites may coexist at pressures 18–22 kbar is differences in their bulk major element compositions because spinel–garnet phase transition takes place at greater depths for more refractory rocks (Klemme and O'Neill, 2000; Nickel and Green, 1985; O'Neill, 1981; Robinson and Wood, 1998; Walter, 2003; Webb and Wood, 1986). For example, garnet–spinel xenoliths 313-37, 314-74 and 314-580 have higher MgO and lower Al₂O₃ than any garnet lherzolite in this study; SP-2 xenolith 314-59 has lower Al₂O₃ and higher MgO and Cr₂O₃ than SP-1 rocks 314-56 and 314-58 (Table 2). In particular, the SP-2 and garnet–spinel peridotites have higher Cr₂O₃/Al₂O₃ (0.12–0.16) than garnet lherzolites (0.08–0.11).

Temperature estimates obtained from analyses of mineral rims for all the xenoliths except the shallow SP-1 peridotites are higher than those obtained from analyses of the cores (Table 1) and appear to indicate heating in the mantle (below the depths where the SP-1 rocks occur) shortly before the transport of the xenoliths to the surface. The same heating event may have caused the formation of kelyphite after garnet (Fig. 3b). The heating affected some samples stronger than others because the width of the zoned pyroxene rims ranges broadly (tens to hundreds of micrometers) as does the width of kelyphite rims (Fig. 2d in Ionov, 2004). Thus the heating was probably uneven and may have been caused by local intrusions of magma. In summary, the mineralogical and P – T data indicate that the CLM beneath Vitim experienced slow isobaric cooling (possibly after the last major crustal magmatic event in Early Mesozoic) followed by

Table 3
EPMA of minerals from Vitim xenoliths

	313-1		313-5			313-3		313-6			313-7					313-8		313-37			313-110
	Opx at pit	Ol av.4	Cpx av.4	Opx av.4	Gar av.4	Opx at pit	Gar av.5	Cpx av.5	Opx av.4	Ol av.4	Opx av.4	Cpx av.4	Gar av.4	Spl av.2	Phl av.2	Opx at pit	Gar at pit	Cpx at pit	Opx at pit	Opx at pit	
SiO ₂	55.30	40.71	52.87	54.96	42.45	55.52	42.01	52.35	54.45	40.60	55.12	52.39	42.39	0.26	36.51	54.97	42.71	52.89	55.86	55.76	
TiO ₂	0.15	0.01	0.51	0.18	0.18	0.15	0.21	0.64	0.18	0.01	0.17	0.54	0.19	0.49	3.52	0.18	0.18	0.39	0.13	0.15	
Al ₂ O ₃	3.78	0.04	6.31	4.62	22.78	3.81	22.74	5.93	4.24	0.03	4.16	5.94	22.91	45.32	13.96	3.89	22.82	5.69	3.92	3.97	
Cr ₂ O ₃	0.51	0.02	1.14	0.62	1.27	0.54	1.37	1.17	0.57	0.03	0.54	1.20	1.18	20.94	0.01	0.52	1.08	1.21	0.54	0.58	
FeO	6.26	9.56	3.25	6.18	7.16	6.31	7.11	3.14	6.19	9.73	6.34	3.34	7.29	13.35	16.73	6.12	7.54	3.23	6.35	6.11	
MnO	0.07	0.13	0.10	0.14	0.33	0.16	0.31	0.10	0.14	0.12	0.12	0.09	0.31	0.12	0.29	0.11	0.30	0.13	0.11	0.11	
MgO	33.32	49.54	15.92	32.39	21.27	33.06	21.05	15.52	32.05	49.05	32.68	15.84	21.03	19.16	12.52	32.86	21.30	16.04	32.95	33.13	
CaO	0.81	0.09	18.00	0.94	4.78	0.80	4.85	18.39	0.89	0.07	0.92	18.06	4.82	0.00	0.12	0.85	4.94	18.45	0.87	0.82	
Na ₂ O	0.10	0.02	2.06	0.21	0.03	0.18	0.04	1.97	0.18	0.01	0.17	1.91	0.03	0.04	0.08	0.16	0.03	1.89	0.14	0.16	
K ₂ O		0.00	0.00	0.01	0.00		0.00	0.01	0.00	0.01	0.01	0.01	0.00	0.00	6.27						
NiO	0.11	0.37	0.04	0.09	0.01	0.09	0.02	0.06	0.10	0.38	0.10	0.04	0.01	0.32	0.11	0.14	0.00	0.07	0.10	0.06	
Total	100.41	100.47	100.20	100.32	100.25	100.62	99.72	99.28	99.00	100.04	100.31	99.37	100.16	100.01	90.11	99.80	100.91	99.98	100.98	100.85	
Mg#	0.905	0.902	0.897	0.903	0.841	0.903	0.841	0.898	0.902	0.90	0.90	0.89	0.84	0.72	0.57	0.91	0.83	0.90	0.90	0.91	
Cr#			0.108	0.082				0.117	0.083			0.08	0.12	0.24	0.00		0.03	0.12	0.09	0.09	

Analyses marked "at pit" were done next to pits produced by laser ablation ICPMS analyses.

Table 3 (continued)

	314-5					314-6	314-6	314-58	314-59	314-74			314-230					314-580	
	Ol av.4	Opx av.4	Cpx av.4	Spl av.4	Phl av.2	Cpx at pit	Opx at pit	Opx at pit	Opx at pit	Gar at pit	Opx at pit	Phl av.2	Ol av.4	Opx av.3	Cpx av.4	Gar av.4	Spl av.2	Opx at pit	Gar at pit
SiO ₂	40.58	54.86	52.62	0.20	38.09	54.20	56.13	54.70	54.56	42.67	54.78	37.06	41.05	55.24	52.83	42.62	0.25	54.70	42.73
TiO ₂	0.01	0.18	0.57	0.53	2.08	0.17	0.05	0.15	0.10	0.21	0.07	2.12	0.01	0.15	0.52	0.14	0.37	0.19	0.20
Al ₂ O ₃	0.03	4.33	6.21	44.52	14.33	3.55	3.31	4.42	4.76	22.74	4.55	15.09	0.04	4.64	6.08	22.69	48.04	4.56	22.56
Cr ₂ O ₃	0.01	0.61	1.18	20.69	0.00	1.15	0.65	0.28	0.47	1.29	0.52	0.00	0.03	0.52	1.03	1.27	18.23	0.60	1.52
FeO	10.49	6.65	3.55	15.18	16.38	2.43	5.58	6.64	6.05	6.89	5.86	20.02	9.60	6.22	3.15	7.21	12.87	6.13	7.17
MnO	0.11	0.13	0.07	0.11	0.64	0.11	0.13	0.13	0.14	0.29	0.14	0.44	0.11	0.15	0.09	0.32	0.07	0.16	0.31
MgO	48.95	32.35	15.30	18.59	12.50	17.31	34.17	32.84	32.63	21.48	32.59	10.81	49.66	32.71	15.79	21.06	19.90	32.14	21.61
CaO	0.07	0.87	18.07	0.01	0.25	20.93	0.76	0.47	0.83	4.76	1.00	0.00	0.09	0.79	18.42	4.82	0.00	1.01	4.78
Na ₂ O	0.01	0.16	2.15	0.00	0.06	0.82	0.09	0.06	0.14	0.03	0.16	0.13	0.02	0.16	1.87	0.02	0.02	0.23	0.05
K ₂ O	0.01	0.00	0.00	0.01	6.02					0.00	0.01	7.70							
NiO	0.36	0.10	0.05	0.31	0.09	0.05	0.10	0.09	0.10	0.02	0.11	0.00	0.39	0.11	0.06	0.00	0.33	0.10	0.01
Total	100.63	100.24	99.77	100.15	90.42	100.75	100.96	99.78	99.77	100.36	99.78	93.37	101.01	100.70	99.82	100.15	100.06	99.81	100.94
Mg#	0.893	0.897	0.885	0.686	0.576	0.927	0.916	0.90	0.91	0.848	0.908	0.490	0.902	0.904	0.899	0.839	0.734	0.903	0.843
Cr#		0.087	0.113	0.238		0.179	0.117	0.041	0.062	0.037	0.072			0.070	0.102	0.036	0.203	0.080	0.043

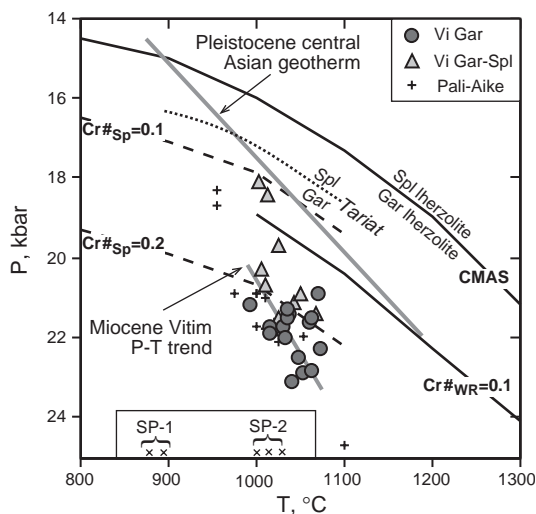


Fig. 6. P – T estimates for Vitim peridotite xenoliths (Table 1) based on the Ca-in-*opx* thermometer of Brey and Köhler (1990) combined with the barometer of Nickel and Green (1985). Black crosses are P – T estimates for xenoliths from Pali-Aike, Patagonia (Kempton et al., 1999b; Stern et al., 1986) calculated for mineral cores using the same methods. Vitim garnet peridotites plot on the Pali-Aike P – T trend. Pleistocene central Asian geotherm is based on data for xenoliths from southern Siberia and central Mongolia (Ashchepkov et al., 1989, 1996; Ionov, 2002; Ionov et al., 1998; Litasov et al., 2000). Solid black lines are transition boundaries between spinel and garnet lherzolites in the CMAS system (Klemme and O'Neill, 2000) and for a lherzolite with whole-rock $Mg\#=0.9$ and $Cr\#=0.1$ (Nickel, 1986). Dashed lines are spinel-to-garnet transition boundaries as a function of $Cr/(Cr+Al)$ in spinel at whole-rock $Mg\#=0.9$ (O'Neill, 1981). Dotted line is a spinel–garnet phase boundary established for fertile lherzolites from Tariat, Mongolia (Ionov et al., 1998). Diagonal crosses (shown out of P scale) next to the T -axis show temperatures for SP-1 and SP-2 spinel peridotites.

rapid localised heating possibly related to Miocene volcanism.

5. Trace element compositions

Trace element compositions of whole-rock xenoliths and mineral separates determined by solution ICPMS are given in Table 4. Analyses of minerals done by LA-ICPMS are given in Table 5. Solution and laser-ablation ICPMS data on some other Vitim xenoliths analysed for Sr–Nd isotopes were published earlier (Ionov, 2004; Ionov et al., in press). This study provides the first reliable dataset on abundances of highly incompatible elements (Th, U, Nb, Ta, LREE)

in garnet and orthopyroxene from Vitim xenoliths and one of the first such datasets for unmetasomatised garnet peridotites worldwide. The data on those elements were either missing or of low precision in LA-ICPMS analyses of garnet and orthopyroxene from Vitim peridotites published earlier (Glaser et al., 1999; Ionov, 2004).

Abundances of highly incompatible elements obtained by whole-rock analyses of the Vitim xenoliths are consistently higher than whole-rock estimates calculated from mineral analyses and modal data (Fig. 7). The difference is greater for less compatible elements (e.g., for Sr than for Nd); significant proportions of those elements in the rocks are therefore hosted by the interstitial material. These results further emphasize the necessity for careful handpicking of pure mineral grains and the use of acid leaching for Sr–Nd isotope analyses (Zindler and Jagoutz, 1986). The inter-granular enrichments in the rocks are most likely related to alteration of the xenoliths during and after their transport to the surface (Ionov, 2004). A thorough inspection of thin sections and mineral separates found no accessory mineral phases of mantle origin that could host the enrichments. Accessory phlogopite present in two samples cannot be responsible for the enrichments in LREE, Sr, Th, U (Fig. 7) because it has lower abundances of those elements than coexisting clinopyroxene (e.g., Ionov et al., 1997; Pearson et al., 2003). Overall, the behaviour of the incompatible elements (including Sm, Nd, Sr) in the Vitim xenoliths has to be assessed from data on major minerals.

The abundances of all trace elements determined in Vitim clinopyroxenes by solution and laser ablation ICPMS are close to each other (Fig. 7). By contrast, the laser ablation analyses of other minerals have yielded systematically lower values for many incompatible elements (La and Sr in garnet; Th, U, Nb and LREE in orthopyroxene; all elements in olivine except Lu, Yb and Zr) than those determined by solution ICPMS on mineral separates (Fig. 7). Similar results were obtained in some other xenolith studies (Eggins et al., 1998; Garrido et al., 2000). One of the reasons for that is that laser ablation runs, which come across fluid or mineral inclusions, can be identified and discarded whereas analyses of bulk mineral separates include all impurities. Sr–Nd isotope compositions of

Table 4
 Solution ICPMS analyses of whole-rock peridotites, pure mineral separates and groundmass from the host volcanic rock

	Garnet peridotites									Gar-Spl perid.		Spinel peridotites						Veins		Host	Ref.sa.		
	313-54				313-105					313-110	314-74	314-56				314-58		314-59		313-103	313-114	87-1	UB-N
	WR	Opx	Cpx	Gar	WR	Ol	Opx	Cpx	Gar	WR	WR	WR	Ol	Opx	Cpx	WR	WR	Cpx	Am	Am	WR	av.10	
Sc	18.7	8.5	26.8	92.3	19.0	1.5	8.2	28.5	110.9	21.4	10.3	13.8	1.4	14.3	63.0	16.6	17.2	59.5	21.2	17.4	15.8	14	
Rb	0.30	0.05	0.02	0.03	0.16	0.016	0.01	0.01	0.03	0.22	0.24	0.20	0.022	0.02	0.02	0.15	0.22	0.01	3.9	7.2	13.4	3.5	
Sr	18.6	0.47	86.4	0.21	14.9	0.034	0.49	78.5	0.16	24.5	16.3	20.5	0.042	0.22	82.0	15.3	16.6	67.0	269	255	722	7.8	
Zr	7.22	1.35	21.00	24.04	6.32	0.041	1.48	19.77	27.03	7.00	4.04	9.00	0.014	1.24	36.0	6.15	6.03	23.19	123	122	246	3.3	
Nb	0.82	0.09	0.80	0.11	0.60	0.019	0.061	0.50	0.071	0.91	1.01	0.72	0.020	0.020	0.18	0.44	0.78	0.49	74.8	35.6	59.6	0.08	
Ba	6.0	0.1	0.1	0.05	5.4	0.013	0.04	0.13	0.044	4.6	25.0	7.3	0.028	0.052	0.03	15.8	4.0	0.1	88.4	84.9	368	26	
La	0.55	0.028	1.54	0.023	0.41	0.0019	0.010	1.03	0.009	0.77	0.76	0.65	0.0031	0.009	1.05	0.26	0.64	1.09	2.34	3.14	25.8	0.33	
Ce	1.35	0.036	4.72	0.084	1.04	0.0037	0.026	3.58	0.075	1.67	1.26	1.43	0.0049	0.021	3.92	0.68	1.56	3.49	8.70	10.38	60.3	0.8	
Pr	0.20	0.011	0.84	0.036	0.17	0.0016	0.008	0.74	0.032	0.24	0.18	0.24		0.004	0.79	0.13	0.22	0.66	1.62	1.97	7.86	0.123	
Nd	0.99	0.055	4.72	0.40	0.83	0.0030	0.048	4.30	0.39	1.07	0.80	1.17	0.0034	0.022	4.79	0.72	1.07	3.80	9.22	10.11	35	0.61	
Sm	0.34	0.030	1.56	0.56	0.28		0.029	1.50	0.57	0.33	0.20	0.39	0.0016	0.018	1.90	0.28	0.32	1.42	2.88	3.14	7.5	0.216	
Eu	0.13	0.013	0.57	0.38	0.12	0.0013	0.013	0.55	0.39	0.13	0.075	0.16	0.0016	0.008	0.81	0.12	0.12	0.59	1.02	1.09	2.42	0.081	
Gd	0.49	0.050	1.69	1.94	0.43	0.0040	0.052	1.68	2.09	0.45	0.26	0.57	0.0040	0.034	2.97	0.43	0.42	2.13	2.99	3.25	6.97	0.32	
Tb	0.090	0.009	0.22	0.50	0.078	0.0008	0.010	0.23	0.54	0.086	0.044	0.10	0.0007	0.010	0.56	0.081	0.075	0.392	0.39	0.43	0.93	0.06	
Dy	0.62	0.063	1.07	4.21	0.54	0.0068	0.071	1.15	4.62	0.63	0.29	0.73	0.0059	0.098	3.89	0.57	0.50	2.71	1.83	2.07	4.88	0.42	
Ho	0.14	0.012	0.16	1.03	0.12	0.0020	0.015	0.18	1.16	0.15	0.063	0.16	0.0022	0.031	0.86	0.13	0.11	0.59	0.26	0.30	0.78	0.097	
Er	0.40	0.037	0.31	3.15	0.34	0.0053	0.040	0.36	3.62	0.49	0.18	0.45	0.0066	0.12	2.45	0.38	0.31	1.67	0.46	0.60	1.73	0.282	
Tm	0.061	0.005	0.034	0.46	0.05	0.0010	0.006	0.04	0.56	0.079	0.027	0.067	0.0014	0.025	0.36	0.057	0.047	0.240	0.041	0.061	0.20	0.043	
Yb	0.40	0.034	0.17	3.05	0.33	0.0047	0.038	0.20	3.66	0.55	0.18	0.44	0.0102	0.22	2.23	0.37	0.30	1.49	0.21	0.30	1.16	0.283	
Lu	0.065	0.005	0.021	0.49	0.055	0.0012	0.006	0.025	0.60	0.099	0.030	0.071	0.0036	0.046	0.35	0.062	0.050	0.235	0.019	0.033	0.17	0.046	
Hf	0.216	0.055	1.00	0.39	0.198	0.0033	0.063	0.99	0.48	0.205	0.116	0.271	0.0027	0.051	1.26	0.195	0.189	0.892	7.54	6.50	5.94	0.122	
Ta		0.003	0.032	0.003	0.03	0.0012	0.007	0.04	0.002	0.047	0.051	0.036	0.001	0.001	0.015	0.013	0.036	0.022	6.65	3.33	3.46	0.015	
Pb	0.10	0.001	0.08	0.02	0.12	0.02	0.04	0.04	0.12	0.22	0.63	0.18	0.04	0.04	0.05	0.21	0.47	0.07	0.59	0.38	4.18	12.8	
Th	0.046	0.002	0.093	0.003	0.034	0.0003	0.002	0.022	0.001	0.075	0.059	0.051	0.0005	0.0006	0.014	0.020	0.069	0.055	0.072	0.095	3.73	0.063	
U	0.021	0.001	0.022	0.006	0.018	0.0004	0.000	0.006	0.003	0.058	0.019	0.017	0.0004	0.0003	0.007	0.012	0.028	0.016	0.017	0.023	0.45	0.06	

See Ionov et al. (1992b) for analytical details. Data for vein amphibole are from Ionov and Hofmann (1995); data for host volcanic rock are from Ionov (2004).

Table 5
LA-ICPMS analyses of minerals in Vitim peridotite xenoliths

Sa. No.	313-1				313-2				313-3					313-5				GOR-132-G		
	Gar1	Gar2	Cpx av.2	Opx av.2	Gar1	Gar2	Cpx av.3	Opx	Gar1	Gar2	Gar av.3	Cpx av.3	Opx	Gar1	Gar2	Cpx av.3	Opx av.2	av.8	r.s.d.	R.V. J-2000
Ti	955	1065	3133	916	775	697	2116	642	1037	1049	1033	3373	972	960	1005	3028	923	1735.9	1%	1740
Sr	0.098	0.106	74.3	0.20	0.065	0.033	36.6	0.24	0.08	0.12	0.105	78.1	0.24	0.139	0.184	88.3	0.53	14.4	1%	15.6
Y	35.3	27.6	3.9	0.23	32.6	24.4	3.12	0.23	45.5	29.0	37.7	3.32	0.23	26.9	31.2	3.89	0.37	13.9	2%	12.7
Zr	24.5	20.2	21.5	1.01	10.3	8.76	9.11	0.61	32.8	22.0	26.3	23.4	1.14	22.1	25.3	22.5	1.66	10.2	2%	10.3
Nb	0.019	0.021	0.18	0.011	0.041	0.029	0.32	0.025	0.019	0.021	0.023	0.17	0.01	0.153	0.166	1.65	0.122	0.065	6%	0.071
La	0.005	0.003	0.89	0.002	0.003	0.002	0.59	0.004	0.002	0.003	0.003	0.92	0.002	0.006	0.007	1.54	0.013	0.087	2%	0.085
Ce	0.048	0.048	3.23	0.012	0.032	0.018	1.54	0.016	0.037	0.049	0.048	3.40	0.013	0.092	0.086	5.20	0.048	0.385	5%	0.38
Pr	0.025	0.026	0.67	0.003	0.014	0.012	0.32	0.003	0.021	0.026	0.024	0.70	0.004	0.039	0.034	0.99	0.011	0.084	3%	0.095
Nd	0.34	0.38	4.30	0.025	0.22	0.19	2.32	0.028	0.35	0.39	0.38	4.47	0.034	0.43	0.42	5.73	0.068	0.70	2%	0.71
Sm	0.52	0.58	1.54	0.018	0.41	0.41	1.05	0.019	0.63	0.56	0.60	1.56	0.021	0.55	0.57	1.79	0.036	0.52	3%	0.52
Eu	0.33	0.35	0.52	0.010	0.29	0.28	0.39	0.009	0.40	0.35	0.37	0.52	0.010	0.36	0.36	0.59	0.015	0.25	2%	0.26
Gd	2.08	1.95	1.70	0.034	1.70	1.67	1.29	0.035	2.40	1.99	2.16	1.63	0.039	1.96	2.05	1.77	0.050	1.27	3%	1.26
Tb	0.56	0.47	0.22	0.007	0.51	0.45	0.18	0.007	0.67	0.48	0.58	0.20	0.006	0.50	0.53	0.22	0.011	0.28	2%	0.28
Dy	5.40	4.17	1.10	0.045	5.00	4.06	0.91	0.046	6.64	4.38	5.58	0.98	0.042	4.34	4.87	1.11	0.071	2.35	3%	2.14
Ho	1.49	1.02	0.15	0.010	1.34	0.95	0.13	0.010	1.76	1.10	1.49	0.14	0.009	1.02	1.17	0.16	0.013	0.55	3%	0.53
Er	4.98	3.21	0.32	0.024	4.45	2.86	0.26	0.023	5.93	3.71	5.05	0.26	0.026	3.09	3.61	0.32	0.035	1.69	3%	1.62
Tm	0.77	0.51	0.03	0.003	0.69	0.41	0.027	0.003	0.92	0.62	0.81	0.03	0.004	0.44	0.54	0.036	0.005	0.256	3%	0.244
Yb	5.48	3.62	0.17	0.023	5.01	2.80	0.14	0.020	6.68	4.55	5.97	0.13	0.026	3.01	3.66	0.18	0.035	1.76	3%	1.61
Lu	0.86	0.58	0.02	0.003	0.76	0.39	0.016	0.0026	1.02	0.74	0.93	0.014	0.004	0.44	0.54	0.021	0.0052	0.26	3%	0.24
Hf	0.45	0.31	0.97	0.042	0.23	0.18	0.58	0.032	0.50	0.35	0.42	1.01	0.045	0.35	0.40	0.92	0.059	0.38	3%	0.37
Ta	b.d.	0.0005	0.02	0.0008	0.001	b.d.	0.028	0.001	0.001	0.001	0.001	0.017	b.d.	0.004	0.005	0.34	0.013	0.030	7%	0.034
Pb	0.006	0.006	0.11	0.0039	0.012	0.007	0.06	0.012	0.008	0.001	0.005	0.105	0.006	0.005	b.d.	0.051	0.008	17.3	4%	21
Th	0.0004	0.0005	0.015	0.0005	0.0011	0.0015	0.034	0.0009	b.d.	b.d.	b.d.	0.013	0.003	0.002	0.003	0.073	0.002	0.0067	13%	0.016
U	0.0013	0.0019	0.005	0.0001	0.0030	0.0021	0.007	0.0005	0.001	0.001	0.001	0.005	b.d.	0.004	0.005	0.015	0.001	0.039	6%	0.045

b.d., below detection. Analyses of garnets with highest and lowest HREE are provided separately if Lu values in individual analyses differ by >20%.

Reference values (R.V.) for MPI-DING glasses are from Jochum et al. (2000). R.s.d., relative standard deviation per cent (one sigma divided by average).

Table 5 (continued)

Sa. No.	KL2-G			313-7				313-8				313-37					314-230			314-5		314-6	
	av.7	r.s.d.	R.V. J-2000	Gar1	Gar2	Cpx av.4	Opx	Gar1	Gar2	Cpx av.2	Opx	Gar1	Gar2	Gar av.3	Cpx av.4	Opx av.2	Gar av.2	Cpx av.3	Opx av.2	Cpx av.2	Opx av.2	Cpx av.2	Opx av.2
Ti	15182	1%	15600	1068	1039	3187	1006	1214	1287	3278	984	857	863	902	2307	778	773	2723	785	3293	1072	791	293
Sr	323	2%	364	0.122	0.159	81.4	0.40	0.12	0.121	87.6	0.35	0.083	0.088	0.086	67.9	0.59	0.087	83.3	0.33	72.5	0.28	30.7	0.07
Y	24.6	1%	26.8	29.6	53.0	4.06	0.34	34.4	39.6	5.95	0.35	39.6	68.8	48.6	3.90	0.30	39.1	5.10	0.35	4.0	0.32	7.01	0.51
Zr	142	1%	159	24.7	31.8	22.2	1.44	32.7	38.4	24.7	1.38	19.8	29.6	22.8	15.7	1.20	20.7	24.1	1.52	30.0	2.36	4.48	0.30
Nb	13.8	2%	15.8	0.082	0.105	0.92	0.052	0.050	0.051	0.68	0.034	0.031	0.040	0.035	0.40	0.056	0.032	0.91	0.047	1.04	0.064	0.046	0.005
La	13.1	2%	13.2	0.008	0.009	1.56	0.006	0.005	0.007	1.49	0.004	0.004	0.005	0.004	0.92	0.021	0.003	1.60	0.006	1.55	0.005	0.43	0.001
Ce	29.9	3%	32.9	0.080	0.075	4.47	0.028	0.061	0.057	5.06	0.021	0.040	0.049	0.044	2.95	0.044	0.049	4.65	0.023	5.73	0.028	1.34	0.005
Pr	4.37	2%	4.71	0.035	0.035	0.79	0.006	0.035	0.029	0.94	0.007	0.018	0.022	0.02	0.57	0.01	0.023	0.83	0.006	1.11	0.008	0.26	0.001
Nd	21.4	2%	21.7	0.43	0.39	4.71	0.046	0.48	0.47	5.47	0.042	0.29	0.27	0.28	3.44	0.05	0.34	4.85	0.043	6.38	0.057	1.61	0.01
Sm	5.53	2%	5.55	0.59	0.54	1.58	0.021	0.70	0.76	1.74	0.023	0.51	0.50	0.51	1.23	0.03	0.57	1.62	0.025	1.95	0.036	0.61	0.01
Eu	1.85	2%	1.95	0.36	0.35	0.53	0.009	0.43	0.47	0.60	0.012	0.33	0.37	0.35	0.43	0.01	0.37	0.56	0.011	0.64	0.014	0.23	0.004
Gd	5.83	1%	6.1	1.99	2.28	1.67	0.055	2.40	2.59	1.90	0.057	2.07	2.52	2.17	1.44	0.05	2.61	2.08	0.053	1.92	0.051	0.89	0.016
Tb	0.87	2%	0.93	0.51	0.68	0.22	0.011	0.60	0.66	0.26	0.010	0.57	0.79	0.62	0.20	0.01	0.68	0.285	0.009	0.25	0.009	0.16	0.006
Dy	5.34	2%	5.35	4.62	7.16	1.12	0.069	5.27	6.02	1.47	0.059	5.52	8.76	6.39	1.05	0.06	6.44	1.52	0.071	1.23	0.067	1.24	0.056
Ho	0.99	1%	0.99	1.11	1.98	0.17	0.012	1.24	1.43	0.24	0.013	1.46	2.63	1.83	0.16	0.01	1.66	0.24	0.016	0.18	0.012	0.27	0.018
Er	2.55	2%	2.64	3.44	6.91	0.35	0.034	3.73	4.41	0.53	0.036	4.77	9.75	6.77	0.34	0.04	5.49	0.51	0.046	0.34	0.033	0.80	0.071
Tm	0.338	2%	0.336	0.53	1.11	0.036	0.006	0.56	0.67	0.06	0.005	0.75	1.72	1.22	0.04	0.01	0.89	0.058	0.007	0.035	0.004	0.11	0.015
Yb	2.14	3%	2.13	3.72	8.31	0.19	0.036	3.95	4.73	0.34	0.043	5.33	13.3	9.92	0.20	0.04	6.36	0.322	0.053	0.17	0.029	0.77	0.136
Lu	0.296	2%	0.296	0.57	1.30	0.023	0.005	0.58	0.70	0.042	0.005	0.80	2.24	1.75	0.02	0.01	0.98	0.037	0.008	0.020	0.0035	0.11	0.024
Hf	3.90	1%	4.14	0.41	0.48	0.98	0.056	0.59	0.65	0.93	0.050	0.32	0.45	0.37	0.73	0.05	0.32	1.04	0.056	1.29	0.068	0.19	0.011
Ta	0.96	2%	0.97	b.d.	0.003	0.036	0.002	0.002	0.002	0.083	0.0015	b.d.	0.0008	0.0017	0.031	0.006	0.001	0.05	0.003	0.27	0.0071	0.009	b.d.
Pb	1.57	4%	2.2	0.01	0.008	0.09	0.002	0.006	0.007	0.054	0.001	0.004	0.006	0.005	0.054	0.006	0.003	0.105	0.003	0.10	0.0063	0.073	0.003
Th	1.02	1%	1.03	0.004	0.003	0.099	0.005	0.0009	0.0012	0.073	0.0033	0.0009	0.001	0.0022	0.033	0.006	0.001	0.087	0.001	0.079	0.0008	0.012	0.0001
U	0.53	3%	0.55	0.008	0.008	0.020	0.001	0.0025	0.0025	0.015	0.0003	0.0016	0.0025	0.0031	0.0079	0.0019	0.002	0.019	0.0007	0.015	0.0005	0.003	b.d.

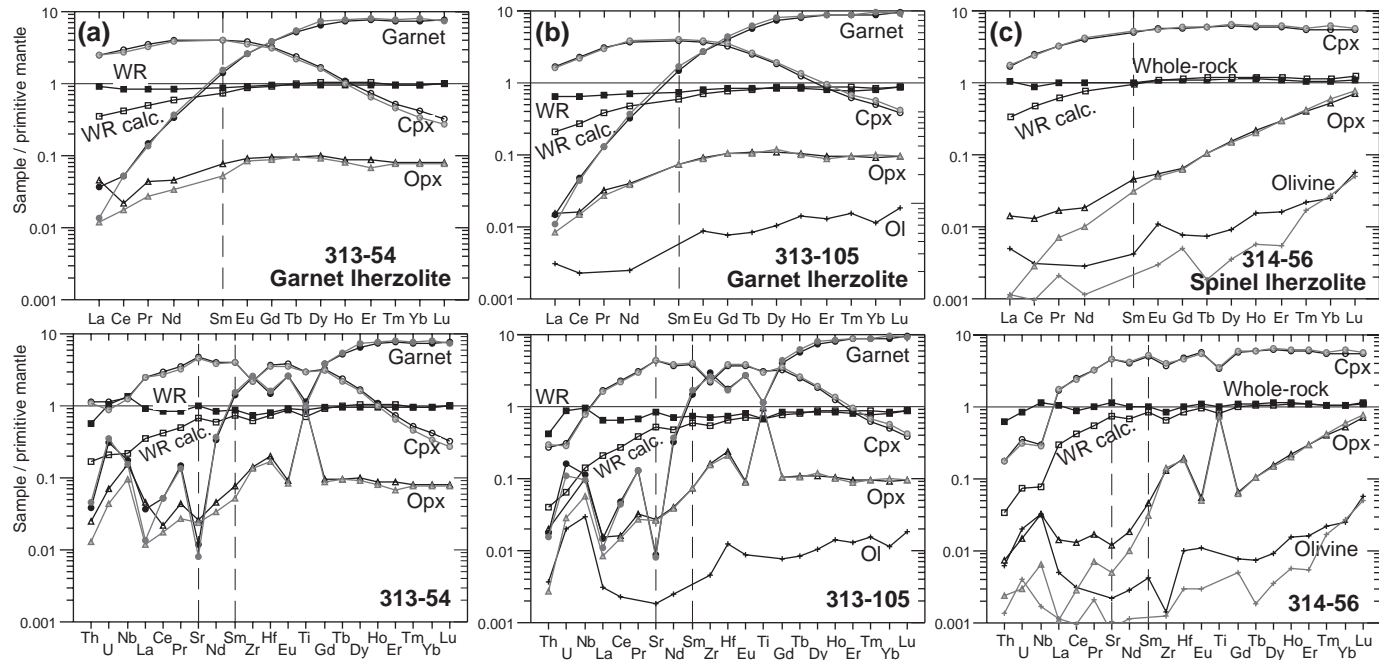


Fig. 7. Primitive mantle-normalized (Hofmann, 1988) element abundance patterns for minerals and whole-rocks (measured and calculated from mineral analyses and modal data) of garnet lherzolites 313-54 and 313-105 and spinel lherzolite 314-56. Solution ICPMS analyses of minerals (Table 4) are shown in black, LA-ICPMS data (Ionov et al., 2005) are in grey.

Vitim minerals were determined on duplicates of the separates analysed by solution ICPMS. Thus, it is important that the concentrations of Sr, Nd and Sm in clinopyroxene and of Nd and Sm in garnet obtained by the two methods are similar whereas Sr concentrations in garnet obtained by LA-ICPMS are systematically lower.

Garnet is the main HREE host in garnet lherzolites (Fig. 7) (Ionov et al., 1993; Kempton et al., 1999a; McDonough and Frey, 1989; Xu et al., 2000). The range of HREE concentrations in Vitim garnets is greater than for MREE and LREE (Fig. 8); garnet grains in many Vitim xenoliths have HREE zoning (Table 5; Ionov et al., in press). The strong partitioning of the MREE and REE into garnet is the reason why the right-hand segments of REE patterns are distinct in pyroxenes from garnet-free and garnet-bearing peridotites (Figs. 7–9). The HREE patterns in clinopyroxene from normal spinel peridotites are nearly flat, with $HREE_{PM} > 1$ (Fig. 9d), while the HREE patterns in clinopyroxene from garnet lherzolites are steep, with $Lu_{PM} \ll 1$ (Fig. 9b). HREE levels in clinopyroxene from peridotites with low modal garnet are intermediate (Fig. 9b). Similarly, HREE abundances in orthopyroxene from spinel peridotites are much higher than in orthopyroxene from garnet-rich peridotites and the slopes of the HREE patterns are distinct (Fig. 9c). The HREE abundances in pyroxenes in xenolith 314-5 are much lower than

those in other spinel peridotites in this study but are similar to those in garnet-bearing xenoliths (Fig. 9c and d). The whole-rock sample of xenolith 314-5 is markedly depleted in heavy relative to middle REE. Ionov (2004) found similar REE patterns in several other spinel peridotites from Vitim and argued that they may have been produced by equilibration with garnet from adjacent garnet-rich rocks in modally heterogeneous mantle.

The share of garnet in the whole-rock budget of individual REE decreases dramatically from Lu to La. The abundances of Sm and Nd in clinopyroxene are several times higher than in coexisting garnet and two orders of magnitude higher than in orthopyroxene for all xenoliths from this study (Figs. 7 and 8). The abundances of Sr in clinopyroxene are 2–3 orders of magnitude higher than in garnet or orthopyroxene. Hence, clinopyroxene is the most important host for Nd and the only significant host for Sr in both garnet and spinel peridotites.

REE patterns of garnet and pyroxenes in the Vitim xenoliths are fairly smooth (Fig. 8), but their extended trace element patterns are more complex (Fig. 9). A major reason for that is that inter-mineral partitioning of some trace elements (in particular, HFSE:Ti, Zr, Hf, Nb and Ta) is distinct from those of adjacent REE with similar general compatibility in the peridotite–melt system (Hofmann, 1988; Sun and McDonough, 1989). Garnets have positive Zr and negative Hf anomalies relative to Sm and Eu (Fig. 9a). By contrast, coexisting clinopyroxenes have negative Zr anomalies (Fig. 9b) while orthopyroxene patterns show spikes for all HFSE, including positive Zr–Hf anomalies (Fig. 9c). As a result, the Zr/Hf and Sm/Zr ratios in coexisting garnet and pyroxenes are distinct. Garnet has positive anomalies of U, Nb and Ta and negative anomalies of Sr, Hf and Ti, and typically very low Th/U ratios (Fig. 9a).

Some apparent ‘anomalies’ in mineral element patterns may be caused by inter-mineral (mainly gar–cpx) partitioning and cannot always be seen as indicative of whole-rock patterns without taking into account the patterns and modal abundances of other minerals. For example, negative Zr and positive Sr anomalies in clinopyroxene from fertile garnet lherzolites (Fig. 9b) are complementary to Zr enrichments and Sr depletions in garnet (and to a lesser degree in orthopyroxene). Negative Ti anomalies in garnet and

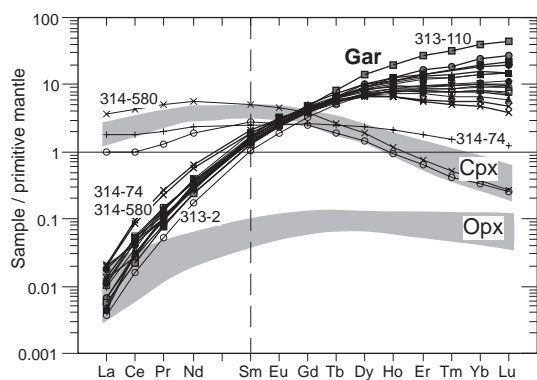


Fig. 8. A summary of primitive mantle-normalized (Hofmann, 1988) REE abundance patterns for minerals in garnet-bearing peridotites from Vitim (LA-ICPMS data from this work and Ionov et al., 2005). Individual patterns are shown for all garnets and for three clinopyroxenes with highest and lowest REE. Compositional fields (grey) are shown for the remainder of clinopyroxenes and for orthopyroxenes.

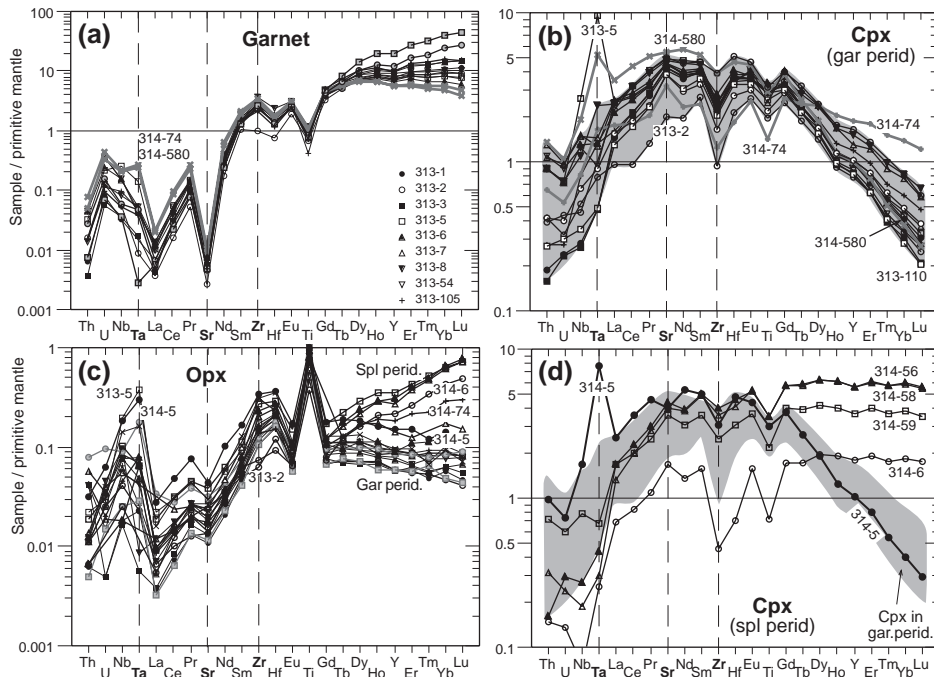


Fig. 9. Primitive mantle-normalized (Hofmann, 1988) element abundance patterns for garnet (a), clinopyroxene (b, d) and orthopyroxene (c). Sample numbers are indicated for all spinel peridotites and selected garnet-bearing xenoliths with extreme compositions. The field of clinopyroxene compositions from garnet-bearing xenoliths (same samples as in Fig. 8) is shown in (d). HREE abundances in pyroxenes from garnet-free xenolith 314-5 are distinct from those in other spinel peridotites and plot in the field for garnet-bearing xenoliths.

clinopyroxene are matched by a Ti spike in orthopyroxene (McDonough et al., 1992; Rampone et al., 1991).

Trace element patterns of clinopyroxene in nearly all spinel and garnet lherzolites show consistently decreasing values from MREE to less compatible LREE, Ta, Nb, U and Th (Figs. 8 and 9b and c). Apart from minor anomalies related to inter-mineral partitioning, these patterns appear to be controlled by cpx/melt partition coefficients ($D^{\text{cpx/melt}}$) and are generally consistent with an origin as partial melting residues. None of the clinopyroxenes shows enrichments in highly incompatible relative to more compatible elements. This absence of significant cryptic metasomatism, even in moderately refractory xenoliths, sets the Vitim peridotite series apart from the majority of other off-craton xenolith suites (Downes, 2001; Frey and Green, 1974; Ionov et al., 2002a; McDonough and Frey, 1989; Pearson et al., 2003).

Nevertheless, evidence for minor metasomatic enrichments can be found in a small number of Vitim

xenoliths. Clinopyroxene 314–580 has markedly higher abundances of LREE–MREE, Sr, Zr and Hf than any other clinopyroxene in this study (Fig. 9b). Clinopyroxene 314-74 has higher LREE/MREE than in other Vitim xenoliths. Garnets from these two samples (314-74 and 314-580) have higher LREE and Ta than other Vitim garnets (Fig. 9a). Clinopyroxenes 314-6, 314-59 and 314-74 have minor positive Sr anomalies. An enigmatic feature of pyroxenes in xenoliths 313-5 and 314-5 are Nb and Ta spikes and low Nb/Ta.

6. Sr–Nd isotope compositions

Sr–Nd isotope data and abundances of Sm, Nd, Rb and Sr determined by ID are given in Table 6. The ID data for clinopyroxene match well those obtained by laser ablation and solution ICPMS (Tables 4 and 5; Ionov et al., in press) except for Sm in cpx-313-2. The ID value for Sm (1.77 ppm) in

Table 6
Sr–Nd isotope data for minerals from Vitim xenoliths and host volcanic rock

Sample number	Sm, ppm	Nd, ppm	¹⁴⁷ Sm/ ¹⁴⁴ Nd	¹⁴³ Nd/ ¹⁴⁴ Nd	2σ × 10 ⁻⁵	Gar–Cp age, Ma	K, ppm	Rb, ppm	Sr, ppm	⁸⁷ Rb/ ⁸⁶ Sr	⁸⁷ Sr/ ⁸⁶ Sr	2σ × 10 ⁻⁵	Sr/Nd
<i>Garnet peridotites</i>													
313-1 Cpx	1.46	4.11	0.215	0.51344	2	30 ± 14	59	0.011	76.9	0.00005	0.70258	2	18.7
313-1 Gar	0.56	0.34	0.989	0.51359	7		2.4	0.002	0.20	0.0026			0.6
313-2 Cpx	/1.77/	2.45	/0.438/	0.51403	2	38 ± 12	47	0.012	41.0	0.0001	0.70238	2	16.7
313-2 Gar	0.44	0.24	1.114	0.51424	5		3.3	0.005	0.54	0.0031			2.3
313-3 Cpx	1.53	4.42	0.209	0.51335	2	39	57	0.006	84.2	0.00002	0.70216	2	19.0
313-3 Gar	0.43	0.27	0.949	0.51354	2		2.1	0.004	0.34	0.0036	0.7049	20	1.2
313-6 Cpx	1.58	4.71	0.203	0.51339	2	40	50	0.006	89.8	0.00002	0.70235	2	19.1
313-6 Gar	0.59	0.41	0.861	0.51356	3		1.3	0.002	0.21	0.0030	0.70299	7	0.5
313-8 Cpx	1.71	5.53	0.188	0.51308	2	28 ± 8	44	0.002	95.2	0.00001	0.70256	2	17.2
313-8 Gar	0.65	0.43	0.904	0.51321	3		2.3		0.25				0.6
313-54 Cpx	1.55	4.72	0.199	0.51339	2	33 ± 6	55	0.006	92.5	0.00002	0.70214	2	19.6
313-54 Gar	0.61	0.41	0.892	0.51354	2		1.5		0.21		0.70437	6	0.5
313-105 Cpx	1.49	4.13	0.218	0.51335	1	27			78.2		0.70226	2	18.9
313-105 Gar	0.61	0.42	0.890	0.51347	1				0.15		0.7024	20	0.4
313-105 Opx	0.03	0.05	0.347						0.54		0.70262	2	10
313-240 Cpx	1.46	4.18	0.212	0.51344	2				82.8		0.70211	1	19.8
<i>Garnet–spinel peridotites</i>													
313-37 Cpx	1.22	3.44	0.215	0.51370	2	39 ± 6	56	0.009	73.8	0.00004	0.70193	2	21.4
313-37 Gar	0.46	0.32	0.885	0.51387	2		2.6	0.004	0.14	0.0088	0.70344	2	0.4
313-110 Cpx	1.49	3.65	0.248	0.51361	1	24	40	0.0005	73.3	0.00002	0.70211	3	20.1
313-110 Gar	0.51	0.29	1.044	0.51374	2				0.16				0.5
314-580 Cpx	1.96	6.27	0.188	0.51317	3		59	0.002	101.4	0.00005	0.70278	1	16.2
314-74 Cpx1	1.03	2.86	0.217	0.51327	2		97	0.1	63.5	0.0046	0.70278	3	22.2
314-74 Cpx2	1.07	3.05	0.212	0.51320	2		90	0.019	65.3	0.0008	0.70283	3	21
<i>Spinel peridotites</i>													
314-6 Cpx	0.61	1.58	0.235	0.51310	2		99	0.0035	33.0	0.00004	0.70402	2	20.9
314-56 Cpx	1.89	4.54	0.252	0.51338	1		23	b.d.	82.6	–	0.70170	2	18.2
314-58 Cpx	1.76	4.13	0.258	0.51338	1		25	0.05	74.2	0.0019	0.70212	2	18.0
314-59 Cpx	1.41	3.63	0.234	0.51317	2		48	0.001	67.6	0.00004	0.70266	3	18.7
<i>Composite garnet peridotites and veins</i>													
313-4 Cpx	2.15	6.42	0.203	0.51277	2	42 ± 6	30	0.002		0.70393	2		
313-4 Gar	0.75	0.47	0.970	0.51298	2		0.9	0.0013	0.184	0.0024	0.70515	2	0.4
313-103 Cpx	2.05	6.21	0.199	0.51298	2	24	11	b.d.	82.7		0.70304	4	13.3
313-103 Gar	0.74	0.54	0.834	0.51308	2				0.70				1.3
313-103 Opx	0.04	0.06	0.331	0.51307	2				0.54		0.7031	10	8.4
313-103 Am	2.90	9.12	0.192	0.51301	2		16140	4.44	346	0.037	0.70325	4	38
313-103 Phl	0.04	0.14	0.159	0.51300	3		96200	76.8	152	1.46	0.70327	2	1127
313-114 Cpx	2.13	6.20	0.208	0.51304	1	33			83.3		0.70303	20	13.4
313-114 Gar	0.75	0.54	0.839	0.51317	2				0.28				0.5
313-114 Am	2.80	8.71	0.194	0.51295	2		13785	7.2	273.1	0.076	0.70354	3	31.3
<i>Host volcanic rock</i>													
87-1 Matrix	8.57	38.4	0.135	0.51289	1		5381	17.7	617	0.083	0.70462	2	16.1
302-36 Bas.	6.00	27.1	0.134	0.51280	1		16450	26.0	379	0.199	0.70409	2	14.0
La Jolla standard				0.51188	1								

Two cpx fractions were handpicked and analysed for sample 314-74. Fraction cp1 has no visible inclusions; fraction cp2 contains visible micro-inclusions. 2σ errors are indicated for garnet–clinopyroxene Sm–Nd age estimates.

that sample is probably erroneous because it is much higher than the duplicated LA-ICPMS data and yields an anomalously high Sm/Nd (0.72). LA-ICPMS values for Sm and Nd in cpx-313-2 (Table 5) are used below instead of the ID data. The ID and ICPMS data for Sm and Nd in garnet match each other very well, but Sr abundances obtained by in situ LA-ICPMS analyses are consistently lower than both the ID and solution ICPMS data on garnet separates (Fig. 10). That indicates that nearly all garnet separates (except the very pure garnet 313-105) contain a significant Sr component that resides not in the mineral lattice but rather in mineral inclusions or micro-cracks.

Nd abundances in garnet (0.24–0.43 ppm) are an order of magnitude lower than in coexisting clinopyroxene (2.4–5.5 ppm) in normal peridotites. Sm/Nd in clinopyroxene range from 0.3 to 0.45 compared to >1 in garnets (Fig. 11a). The higher Sm/Nd in the garnets are matched by more radiogenic $^{143}\text{Nd}/^{144}\text{Nd}$ than in coexisting clinopyroxenes (Fig. 11b). Sm–Nd isochron ages calculated for garnet–cpx pairs from individual xenoliths range from 24 to 42 Ma (Table 6; Fig. 12a). The lowest of these values approach the likely eruption age of the host volcanic rock (15–18

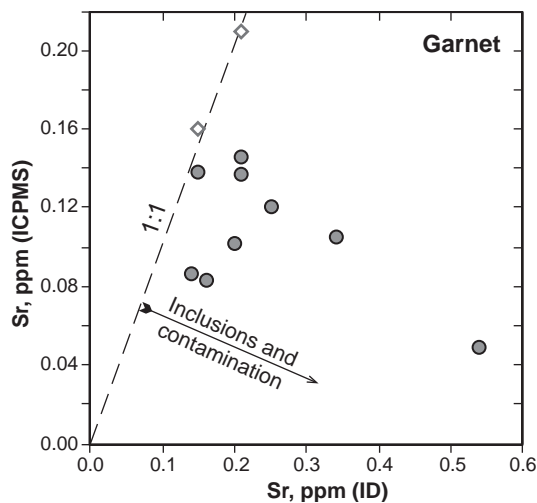


Fig. 10. A plot of Sr (ppm) in garnet separates determined by isotopic dilution (Table 6) versus Sr in garnet from laser ablation (black circles) and solution (grey rhombs) ICPMS. Consistently lower Sr abundances obtained by LA-ICPMS indicate that nearly all garnet separates contain an important contribution from inclusions or grain contamination.

Ma). The differences between the eruption age and the consistently higher garnet–cpx ages appear to indicate that garnet and clinopyroxene in the xenoliths were not in complete isotopic equilibrium at the time of eruption, possibly due to insufficiently rapid diffusional exchange (Van Orman et al., 2001, 2002) in these coarse-grained rocks with irregularly distributed garnet (Figs. 2 and 3). An additional factor that may have contributed to the high garnet–cpx age (42 Ma) for composite xenolith 313-4 is a possible Nd-isotope disequilibrium between its garnet-rich portion and the remainder of the sample.

Garnet–cpx Sm–Nd ages for two veined peridotites (24 and 33 Ma) are consistent with the age estimates for the other xenoliths. By contrast, the Sm–Nd age estimates from amphibole–cpx pairs for those two samples are not meaningful (–0.6 and 0.9 Ga). Garnet and pyroxenes handpicked from 2- to 4-cm-thick slabs with veins in the middle cut from those composite xenoliths originate mainly from their peridotite portions because garnet does not normally occur in the veins while vein clinopyroxene forms small cloudy grains (Fig. 3d), which were rejected during hand-picking in favour of large, clear, inclusion-free clinopyroxene from host peridotite. Hence, the Nd isotope data indicate that the vein amphibole is not in isotopic equilibrium with their host peridotite within about 2 cm distance from the vein centre.

$^{87}\text{Sr}/^{86}\text{Sr}$ in vein amphibole and phlogopite from xenolith 313-103 are within analytical error of each other in spite of a big difference in their $^{87}\text{Rb}/^{86}\text{Sr}$ (0.04 vs. 1.46). Assuming that the two minerals were in isotopic equilibrium ($^{87}\text{Rb}/^{86}\text{Sr}=0.70325$) at the time of eruption (16 Ma), the $^{87}\text{Sr}/^{86}\text{Sr}$ value of the phlogopite must have increased to 0.7036 instead of measured 0.70327. A possible explanation is that phlogopite precipitated in a separate metasomatic episode shortly before the eruption and was not in equilibrium with amphibole.

Rb abundances in clinopyroxene and garnet are very low (typically <0.01 ppm) but garnet has higher $^{87}\text{Rb}/^{86}\text{Sr}$ because its Sr abundances are nearly three orders of magnitude lower than in clinopyroxene. $^{87}\text{Sr}/^{86}\text{Sr}$ values measured in the garnets are higher than for coexisting clinopyroxene, but the differences between the two minerals vary greatly (Table 6). We do not ascribe any specific age significance to those differences because Rb is not likely to reside in crystal

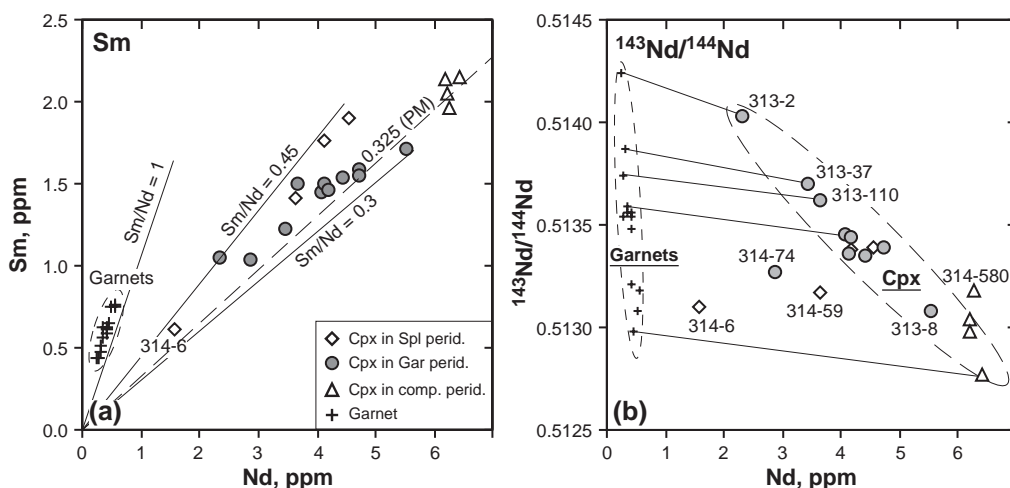


Fig. 11. Plots of Sm vs. Nd abundances (a) and of Nd vs. $^{143}\text{Nd}/^{144}\text{Nd}$ (b) in clinopyroxene (circles, garnet-bearing peridotites; rhombs, spinel peridotites; triangles, veined and metasomatised xenoliths) and garnet (crosses) in Vitim xenoliths. Thin grey lines connect coexisting garnet and clinopyroxene in selected samples.

lattice, and also because the measured Rb/Sr and $^{87}\text{Sr}/^{86}\text{Sr}$ may be strongly affected by the amount of kelyphite and other impurities in the garnet separates. As shown above, a significant proportion of Sr in the separates may be hosted by impurities as well (Fig. 10). The share of Sr residing in garnet is usually <0.3% of that hosted by clinopyroxene (from ID data

in Table 6). Because the total share of Sr in the rock hosted by garnet, orthopyroxene and olivine is $\ll 1\%$ (e.g., Table 4; Fig. 7) we choose not to take into account our $^{87}\text{Sr}/^{86}\text{Sr}$ data on garnet and orthopyroxene in the whole-rock budget and assume that “pre-eruption” whole-rock $^{87}\text{Sr}/^{86}\text{Sr}$ values are identical to those in pure clinopyroxene separates.

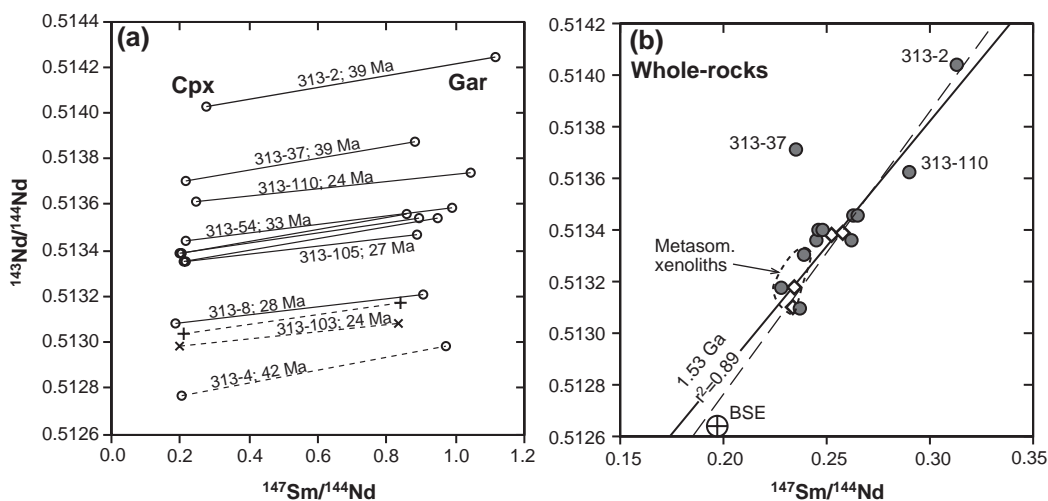


Fig. 12. Plots of $^{147}\text{Sm}/^{144}\text{Nd}$ vs. $^{143}\text{Nd}/^{144}\text{Nd}$ for Vitim xenoliths: (a) garnet–cpx pairs; (b) whole-rock compositions calculated from mineral analyses and modal abundances (Table 7). Clinopyroxene and garnet in each sample are connected with dashed lines and with solid lines for other xenoliths; internal bi-mineral isochron ages (Table 6) are indicated for selected samples. BSE, model bulk silicate Earth (Zindler and Hart, 1986). Dashed line in (b) is linear correlation calculated excluding anomalous sample 313-37; solid line is linear correlation calculated excluding metasomatised samples and including BSE.

By comparison, the share of Nd residing in garnet in fertile lherzolites (5–10%) is much higher than for Sr and cannot be neglected. The share of Sm hosted by garnet is even higher (17–26%), with Sm/Nd much higher than in clinopyroxene. Precise estimates of garnet and clinopyroxene modal abundances are therefore essential in order to obtain meaningful whole-rock age estimates. Whole-rock Sm/Nd and $^{143}\text{Nd}/^{144}\text{Nd}$ calculated from mineral data (Table 6) and modal compositions of Vitim peridotites (Table 1) are given in Table 7.

Clinopyroxenes from the majority of the xenoliths yield a negative linear correlation on a plot of Nd versus $^{143}\text{Nd}/^{144}\text{Nd}$ (Fig. 11b). Because Nd is highly incompatible during partial melting of garnet and spinel facies peridotites (Fig. 13) this correlation is

Table 7
Model Sm–Nd and Rb–Sr depletion ages for whole-rock Vitim xenoliths

Sample number	$^{147}\text{Sm}/^{144}\text{Nd}$ wr-calculated	$^{143}\text{Nd}/^{144}\text{Nd}$ wr-calculated	Sm–Nd model age, PM	Rb–Sr model age, PM
<i>Garnet peridotites</i>				
313-1	0.280	0.51345	1.84	1.73
313-2	0.467	0.51404	1.85	1.90
313-3	0.245	0.51336	2.31	2.07
313-6	0.250	0.51340	2.39	1.91
313-8	0.235	0.51309	1.73	1.74
313-54	0.248	0.51340	2.28	2.08
313-105	0.266	0.51336	1.69	1.98
313-240	0.262	0.51345	1.9	2.10
Average	2.0	± 0.3	1.9	± 0.2
<i>Spinel peridotites</i>				
314-6	0.235	0.51310	1.83	/0.55/
314-56	0.252	0.51338	2.05	2.43
314-58	0.258	0.51338	1.84	2.14
314-59	0.234	0.51317	2.16	1.66
Average:			2.0 ± 0.2	2.1 ± 0.4
Average (gar and spl peridotites)			2.0 ± 0.2	2.0 ± 0.2
<i>Garnet–spinel peridotites</i>				
313-37	0.240	0.51371	4.3	2.26
313-110	0.305	0.51362	1.6	2.10
314-74	0.253	0.51330	2.3	1.57
314-580	0.226	0.51317	2.6	1.56

Ages are calculated relative to primitive mantle values after Zindler and Hart (1986). Values in italics are rough estimates because data for garnet are missing or of low precision.

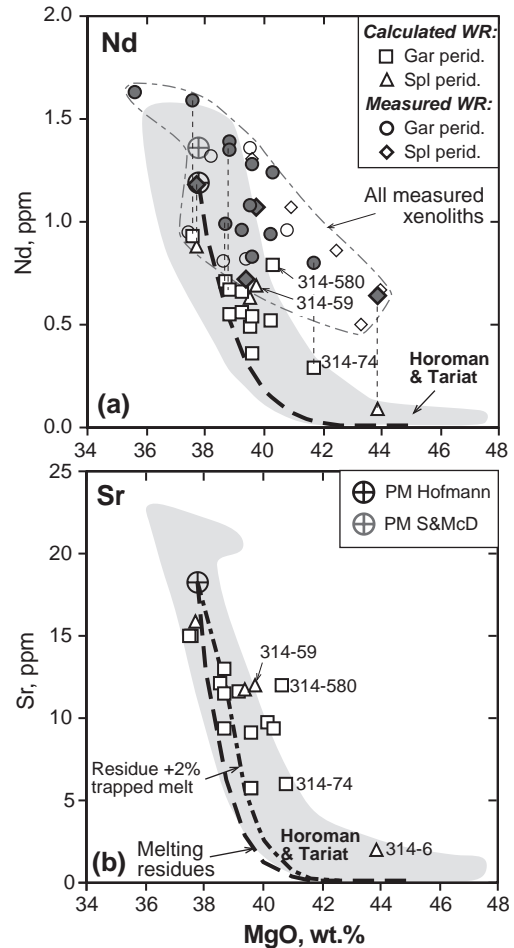


Fig. 13. Co-variation plots for Nd (a) and Sr (b) in ppm vs. MgO (wt.%) for whole-rock Vitim peridotite xenoliths. Empty squares and triangles show abundances of Nd and Sr calculated from mineral analyses and modal data for xenoliths analysed for Sr–Nd isotopes. Circles and rhombs are whole-rock analyses for Nd (filled black symbols are samples analysed for Sr–Nd isotopes, empty grey symbols are other samples). Grey dashed line contours the field of all measured whole-rock compositions from this work and Ionov (2004). Black dashed lines show model compositions of residues after fractional partial melting (1–23%) of primitive mantle (Hofmann, 1988) in spinel and garnet facies (modal garnet before melting is shown) calculated using an algorithm and partition coefficients from Takazawa et al. (2000). The diagram for Sr also shows melting residues with 2% of trapped melt. Grey circle with a cross is primitive mantle composition after Sun and McDonough (1989). Measured and calculated data points of several samples are connected with dashed lines in (a).

likely to be a result of time-integrated evolution of the Sm–Nd system in a series of partial melting residues. Clinopyroxenes that plot off the correlation in Fig.

11b show trace element evidence for metasomatism or re-equilibration with percolating melts (Fig. 9b and d). The Sm–Nd isotope systematics for clinopyroxene alone cannot be used for age estimates because most of the xenoliths contain garnet. Whole-rock $^{143}\text{Nd}/^{144}\text{Nd}$ and $^{147}\text{Sm}/^{144}\text{Nd}$ values calculated from Sm–Nd isotope data for clinopyroxene and garnet and modal abundances (Table 7) are plotted in Fig. 12b. The highly radiogenic Nd isotope compositions of the majority of the peridotites reflect ancient depletion of their lithospheric source in incompatible elements. A linear fit to all whole-rock compositions except sample 313-37, which is an obvious outlier, corresponds to an age of 1.5 Ga and initial ϵ_{Nd} of 3 ($r^2=0.89$). Linear fits forced through the bulk silicate earth point (BSE; Zindler and Hart, 1986) as partial melting source yield good correlations ($r^2\sim 0.92$) and somewhat older ages (1.7–1.8 Ga, depending on whether metasomatised xenoliths, i.e. outliers in Figs. 8 and 11b, are included). Garnet–spinel xenoliths 313-37 and 313-110 deviate most from the linear regression lines because of difficulties in estimating whole-rock Sm/Nd in those samples with irregularly distributed garnet (Ionov et al., in press).

The majority of the Vitim xenoliths plot beyond the field of oceanic basalts on a Sr–Nd isotope diagram (Fig. 14). This is mainly because of the highly radiogenic Nd isotope compositions; two xenoliths also have less radiogenic $^{87}\text{Sr}/^{86}\text{Sr}$ than MORB. Several Vitim xenoliths also have higher $^{176}\text{Hf}/^{177}\text{Hf}$ than MORB (Ionov et al., in press). Many Vitim peridotites with $^{143}\text{Nd}/^{144}\text{Nd}$ higher than in MORB fall within the model DMM reservoir of Zindler and Hart (1986); three xenoliths have even higher $^{143}\text{Nd}/^{144}\text{Nd}$. Three other samples are displaced to the right of the mantle array and appear to be enriched in radiogenic Sr; two of them show trace element evidence for metasomatism (Figs. 9 and 11b). The origin of such displacements in mantle peridotites was recently reviewed by Ionov et al. (2002b). Veined Vitim xenoliths plot in the middle of the mantle array close to the overlap of the OIB and Pacific MORB fields. Volcanic groundmass handpicked from the host Miocene tuff (sample 87-1) plots at the upper margin of the OIB field. Its composition is distinct from that of basalt 302-36 (Table 6) from a nearby Pleistocene eruption centre, which plots close to the middle of the OIB field within a tight cluster formed by several

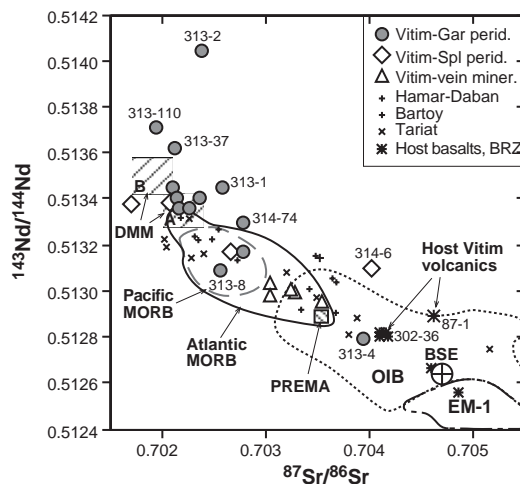


Fig. 14. Plot of $^{87}\text{Sr}/^{86}\text{Sr}$ vs. $^{143}\text{Nd}/^{144}\text{Nd}$ for Vitim xenoliths (clinopyroxene data for spinel peridotites, calculated whole-rock values for garnet peridotites) and host volcanic material. Also shown are compositions of clinopyroxenes in spinel peridotite xenoliths from Bartoy and Hamar-Daban in the Baikal region (Ionov et al., 1992a, 1995) and Tariat in central Mongolia (Stosch et al., 1986), bulk silicate Earth (BSE), prevalent mantle (PREMA) and model depleted mantle (DMM A and B) after Zindler and Hart (1986). Fields of MORB, ocean island basalts (OIB) and enriched mantle (EM-1) are after Hofmann (1997).

other Cenozoic basalts from southern Siberia (Ionov et al., 1992a, 1995). This may indicate that the parental magmas of the Miocene and the younger volcanic rocks had distinct Sr–Nd isotope compositions. On the other hand, sample 87-1 may contain, in spite of handpicking and mild acid leaching, a radiogenic $^{87}\text{Sr}/^{86}\text{Sr}$ component of post-eruption origin. The latter is consistent with a positive Sr anomaly found in the groundmass by solution ICPMS analyses (Ionov, 2004).

The majority of Vitim lherzolites, in particular garnet-bearing samples, have higher $^{143}\text{Nd}/^{144}\text{Nd}$ than spinel lherzolites from two other xenolith suites in southern Siberia (Bartoy and Hamar-Daban; Ionov et al., 1992a, 1995) and from the Tariat locality in nearby central Mongolia (Stosch et al., 1986) whereas their $^{87}\text{Sr}/^{86}\text{Sr}$ mainly overlap (Fig. 14). Very few Vitim peridotites, apart from veined xenoliths, plot in the OIB field, compared to a relatively large proportion of OIB-type xenoliths in the other central Asian localities. It is not clear whether the differences in Nd isotope composition are somehow related to the deeper origin (presence of garnet) of many of the

Vitim xenoliths or are due to large-scale mantle heterogeneities. However, these differences are consistent with the generally very low degrees of metasomatism in the majority of the Vitim samples in this study (see previous section) and the low proportion of metasomatised rocks in the Vitim Miocene xenolith suite in general.

7. Discussion

7.1. The origin of the Vitim peridotite series by partial melting

The majority of the Vitim peridotites plot on the MgO–Al₂O₃ diagram (Fig. 4a) close to the model shallow partial melting trend of Niu (1997) and also within the combined field of spinel peridotites from Tariat (central Mongolia) and Horoman. The Tariat data are used here as an example of a generally fertile xenolith suite in the vicinity of Vitim (Ionov et al., 1998; Press et al., 1986) while the Horoman peridotites represent well-documented residues of moderate to high degrees of polybaric partial melting from a primitive mantle source (Takazawa et al., 2000); both peridotite suites are poorly metasomatised. Regardless of minor scatter around the melting trends, the modal and major element compositions of the Vitim peridotite xenoliths (Figs. 4 and 5), together with REE patterns (Ionov, 2004), are consistent with an origin by shallow partial melting with different (but generally low) degrees of melt extraction from a fertile protolith. A few fertile garnet-bearing Vitim peridotites plot either above or below the combined Tariat–Horoman field (Fig. 4a). The scatter of Al contents for at least some of the Vitim xenoliths may be due to variations in modal garnet abundances, either because of sampling problems related to heterogeneous distribution of coarse garnet (Fig. 2; Palme and O'Neill, 2003) or because of “metamorphic differentiation” during the spinel–garnet phase transition in melting residues on cooling (Ionov, 2004; Ionov et al., in press).

After the original partial melting event or a series of events, the residual peridotites must have been initially spinel facies rocks because garnet is not stable in peridotites at solidus temperatures in the depth range (<80 km) where the xenoliths were entrained in the host magma. As discussed above,

garnet stability, in addition to *P–T* conditions, is strongly dependent on the whole-rock Al contents and Cr/(Cr+Al) values (Klemme and O'Neill, 2000; Nickel, 1986; O'Neill, 1981; Robinson and Wood, 1998; Webb and Wood, 1986). As the mantle in the depth range 60–75 km (18–23 kbar) cooled down, garnet became stable and formed in rocks with high Al and low Cr/(Cr+Al), but not in more refractory rocks. As a result, the cooling produced a mineralogically heterogeneous suite of fertile garnet lherzolites coexisting with less fertile garnet–spinel and spinel peridotites (see also Ionov et al., in press).

As noted by Palme and O'Neill (2003), the contents of FeO in the Vitim peridotites show no apparent correlation with MgO. This inference is also valid with the new major element dataset from this study, which yields a median FeO value of 8.16% (Table 2; Fig. 4b). If three samples with unusually high FeO ($\geq 8.8\%$, possibly related to metasomatism) are discarded, a vague trend of depletion in FeO at higher MgO is outlined, even though the number of MgO-rich rocks is insufficient to establish that trend with certainty (Fig. 4b). Experimental evidence and studies of mantle peridotites indicate that residues of partial melting at 1–2.5 GPa show no or only minor depletion in FeO with the degree of melting (Niu, 1997; Walter, 2003), by contrast with strong depletion in FeO at >3 GPa. Thus, the majority of Vitim peridotites with >40% MgO plot in the field of the Horoman peridotites, which was shown to be formed by shallow partial melting (1–2.5 GPa; Takazawa et al., 2000). Hence, it is most likely that the Vitim xenolith suite was formed by shallow (possibly ~2 GPa) partial melting.

7.2. Average composition of the Vitim peridotite series

Major element compositions of several fertile Vitim xenoliths are similar to those inferred for the primitive mantle (McDonough and Sun, 1995; Palme and O'Neill, 2003); some of the xenoliths have even higher Ca and Al contents (Fig. 4a). On the other hand, moderately refractory peridotites with <3% Al₂O₃ (mostly spinel and garnet–spinel rocks) are common as well. The average and median compositions for the Vitim peridotite suite calculated from data on 29 xenoliths from this study and earlier work (excluding veined and composite samples) are given

in Table 2. The median contents of Al_2O_3 (3.38%), CaO (2.95%) and other major oxides indicate only moderate depletions in “basaltic components” relative to primitive mantle estimates and are similar to averages reported earlier for Vitim xenoliths from the Miocene tuff and younger basalts (3.5% Al_2O_3 , 2.9% CaO; Ionov, 2002). The median and average major oxide values for the Miocene Vitim suite are also similar to averages for several other xenolith suites (mostly consisting of spinel peridotites) from the Baikal region and nearby central Mongolia. Thus, the CLM in the Vitim area may be considered as part of a large-scale fertile lithospheric mantle domain south of the Siberian craton (Ionov, 2002).

A much more fertile median composition for Vitim peridotite xenoliths (4.0% Al_2O_3 , 3.2% CaO) was reported by Griffin et al. (1999) and repeated in several later publications of the same team (Griffin et al., 2003; Poudjom Djomani et al., 2001) as typical of the CLM in “young extensional intraplate terrains”. Two publications (Press et al., 1986; Wiechert et al., 1997) quoted in Table 1 of Griffin et al. (1999) as data sources used to obtain median values for “gt lherz. Siberia/Mongolia” or “Vitim lherzolite xenoliths” contain neither data on xenoliths from Siberia nor data on garnet lherzolites. Two other papers (Griffin et al., 1998; Ionov et al., 1993) from the reference list of Griffin et al. (1999) do contain data on Vitim xenoliths (mainly earlier data on samples from this study). However, median values for Al_2O_3 (3.62%) and CaO (3.04%) calculated from data on 17 garnet-bearing Vitim xenoliths from Griffin et al. (1998) are not as high as those given by Griffin et al. (1999). Furthermore, it is not correct to estimate compositions of CLM sections containing a significant proportion of spinel peridotites based uniquely on garnet-bearing lherzolites because it introduces a sampling bias to more fertile compositions. For example, the median Al_2O_3 obtained in this study for garnet-bearing Vitim peridotites (3.52%) is much higher than for spinel peridotites (2.87%). Thus, the very high median Al_2O_3 and CaO for Vitim xenoliths provided by Griffin et al. (1999, 2003) and Poudjom Djomani et al. (2001) are inconsistent with results of this study and other published data. Griffin et al. (1999) also provide an estimate of CLM composition for the Vitim area based on “garnet xenocrysts in alkali basalts” without reporting the data on the xenocrysts or indicating the

source of the data. Interestingly, an earlier paper (Griffin et al., 1998) reported a summary of EPMA and proton probe data on 30 grains taken at random from several garnet separates used in this study for TIMS and ICPMS analyses. Those garnets come from a small number of fertile, garnet-rich lherzolites and thus cannot be representative of the garnet population in the Vitim CLM. Without addressing the validity or precision of the methods used by Griffin et al. (1999) to assess lithospheric compositions from garnet data, we note that those authors did not demonstrate that their suite of “garnet xenocrysts” from Vitim is representative of the CLM section in the area.

7.3. Trace element evidence for melting and metasomatism

An important issue for the interpretation of radiogenic isotope data on the Vitim peridotites is whether the concentrations of the parent–daughter elements are controlled by partial melting alone or were also affected by later processes, like metasomatism. To address that question whole-rock abundances of Nd and Sr are plotted in Fig. 13 versus MgO as a partial melting index. “Pre-eruption” whole-rock abundances of Nd and Sr were estimated from modal data (Table 1) and isotope dilution analyses of minerals (Table 6), supplemented by ICPMS data if the ID values are not available. The diagram in Fig. 13a further demonstrates that the calculated whole-rock abundances of Nd are significantly lower than the measured values for nearly all samples. The calculated Nd values typically plot near the trends calculated for partial melting residues using established partition coefficients (same as in Ionov et al., 2002a, in press). The latter is valid for melting both in spinel and garnet lherzolite facies fields because garnet/melt partition coefficients ($D^{\text{gar/melt}}$) for Nd and Sr are not higher than $D^{\text{cpx/melt}}$, and therefore the bulk $D^{\text{solid/melt}}$ values are mainly controlled by those for clinopyroxene. Nearly all calculated xenolith compositions plot above the MgO–Sr pure fractional melting trend but they comply much better with a trend assuming 2% residual porosity because trapped melt effects play a greater role for elements with low D values (e.g., Hellebrand et al., 2002; Ionov et al., 2002a). Calculated compositions of several samples (314-6, 314-59, 314-74 and 314-580 marked in Fig. 13) plot

farther off the melt extraction trends than those for the remainder of the xenoliths. As discussed above, it is possible that those samples have been affected by cryptic metasomatism (enrichments in incompatible elements hosted by main minerals).

7.4. Lithospheric age constraints from radiogenic isotope data

As discussed above, chemical data indicate that the Vitim xenoliths were originally formed as residues after melt extraction. The REE+Sr patterns in the majority of those samples appear to preserve the record of a melting event (Figs. 8 and 9). The age of that event (or a series of events) may, therefore, be constrained from the Sm–Nd and Rb–Sr systems. Whole-rock Sm–Nd isotope data overall indicate a Proterozoic age for the melting event but do not yield a good isochron, mainly because of a wide data scatter for three most depleted xenoliths (Fig. 12). Two of them (313-37 and 313-110) are heterogeneous garnet–spinel rocks, with a range of modal garnet and MREE–HREE abundances in garnet (Ionov et al., in press). Whole-rock $^{147}\text{Sm}/^{144}\text{Nd}$ estimates for those samples calculated from mineral analyses and modal data are not precise. On the other hand, modally homogeneous depleted garnet lherzolite 313-2, which has the highest $^{143}\text{Nd}/^{144}\text{Nd}$ in this study, plots on a 1.7 Ga isochron for unmetasomatised Vitim xenoliths (Fig. 12b). The latter correlation extends close to modern BSE composition, which can be seen as evidence that pre-melting protolith for the Vitim peridotite suite was similar in Nd isotope composition to primitive mantle (PM). Sm–Nd model ages relative to PM for whole-rock spinel and garnet lherzolites from Vitim range from 1.7 to 2.4 Ga, with an average of 2.0 ± 0.2 Ga (Table 7). Garnet–spinel peridotites (including two samples that appear to be metasomatised) show a wider scatter of Sm–Nd model ages (1.6 to 4.3 Ga).

Rb is much less compatible than Sr, Nd and Sm and is only present in negligible amounts in pyroxenes, garnet, olivine and spinel. Even small amounts of partial melting of primitive mantle will exhaust Rb in the residue if melt extraction is complete and no potential mineral hosts for Rb, like amphibole and phlogopite, remain in the residual peridotite (Stosch et al., 1986). Therefore, the Rb–Sr system records the

first such depletion event, even if Sr isotope data on ‘anhydrous’ mantle peridotites are not likely to yield isochrons (because Rb/Sr ~ 0 in all minerals). Rb–Sr model ages relative to PM for garnet and spinel Vitim peridotites (except refractory spinel peridotite 314-6) range from 1.7 to 2.4 Ga, with an average 2.0 ± 0.2 Ga; spinel–garnet xenoliths yield model ages of 1.6–2.3 Ga (Table 7). Remarkably, both the overall range and average values of PM model ages for spinel and garnet peridotites from Vitim are identical for the Rb–Sr and Sm–Nd systems. This similarity further demonstrates the poor development of cryptic metasomatism (which particularly affects Sr) in the Vitim suite and is an important piece of evidence for the Paleoproterozoic age (most likely ~ 2 Ga) of depletion events that originally formed the CLM in the Vitim region.

Re–Os isotope data have been reported by Pearson et al. (1998, 2003, 2004) for 16 Vitim xenoliths from the Miocene tuff including 13 samples from this study. Rhenium depletion (T_{RD}) ages for two most refractory peridotites (314-5 and 314-6) are 1.8–1.9 Ga (Fig. 15); rhenium model (T_{MA}) age for sample 314-5 is 2.2 Ga. The T_{RD} and T_{MA} values are considered as minimum and max-

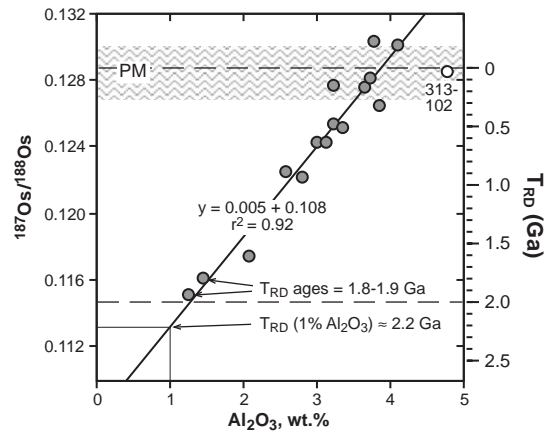


Fig. 15. Al_2O_3 – $^{187}\text{Os}/^{188}\text{Os}$ co-variation diagram for Vitim xenoliths from Miocene tuff. $^{187}\text{Os}/^{188}\text{Os}$ are from Pearson et al. (2004). Al_2O_3 values are same as in Fig. 4a. T_{RD} ages are calculated relative to present-day Bulk Earth (primitive mantle) using $^{187}\text{Os}/^{188}\text{Os}_{\text{BE}}=0.1287$; $^{187}\text{Re}/^{188}\text{Os}_{\text{BE}}=0.4243$; $\lambda^{187}\text{Re}=1.666 \times 10^{-11} \text{ a}^{-1}$ after Shirey and Walker (1998). The shown linear correlation was calculated without sample 313-102, which has unusually high Al_2O_3 (well above that in primitive mantle; Palme and O'Neill, 2003).

imum depletion ages, respectively, because the former assumes no Re in the sample while the latter (based on measured Re/Os) may be affected by Re contamination and the loss of Os after xenoliths were captured by host magma. Importantly, the modal and major oxide compositions of the two samples with most ancient Re–Os ages plot on melt extraction trends defined by the remainder of the xenoliths (Fig. 4); their microstructures are similar to those in other SP-2 Vitim xenoliths. In particular, there are no reasons to consider those samples as remnants of ancient cratonic mantle within younger asthenospheric material because they do not have high modal orthopyroxene typical of peridotites from the nearby Siberian craton (Fig. 5). Furthermore, the $^{187}\text{Os}/^{188}\text{Os}$ in the Vitim peridotites show good linear correlations with Al_2O_3 ($r^2=0.92$; Fig. 15), MgO ($r^2=0.88$; not shown) and other partial melting indices (Pearson et al., 2004). Those correlations appear to indicate that all the xenoliths experienced partial melting at about the same time and at similar conditions.

It was suggested (Reisberg and Lorand, 1995) that the extrapolation of the $\text{Al}-^{187}\text{Os}/^{188}\text{Os}$ trend ('alumichron') to the intercept ($\text{Al}_2\text{O}_3=0$) may give the initial $^{187}\text{Os}/^{188}\text{Os}$ at the time of melting. As discussed earlier by Handler et al. (1997), Pearson (1999) and Pearson et al. (2002), that procedure is unlikely to yield valid age information because Re concentration in partial melting residues may approach zero while they still contain Al-bearing phases. The lowest Al_2O_3 contents found in off-craton xenoliths from central Asia are 0.5–0.8% (Ionov, 2002), consistent with experimental data on residues of high-degree shallow partial melting (Walter, 2003). Moreover, it is unlikely (unpublished petrographic and major-element data of DAI and IA) that highly refractory rocks (<1% Al_2O_3) are present in the Vitim peridotite suite. The intercept of the Vitim 'alumichron' with $\text{Al}_2\text{O}_3=1\%$ yields $T_{\text{RD}}\sim 2.2$ Ga (Fig. 15). Overall, the Re–Os depletion ages are similar to those obtained in this study from the Sr–Nd isotope data. Collectively, they clearly indicate a Paleoproterozoic age for the depletion event. The xenolith ages are not related to their depths of origin arguing against a lithospheric origin by slow downward growth on cooling. The Vitim CLM is not chemi-

cally stratified either and thus shows no evidence for replacement of the lower part of a hypothetical ancient refractory lithosphere by a younger fertile material.

7.5. Lithospheric evolution and crust–mantle coupling in the Vitim area

Little is known about the formation and evolution of the early crust of the Vitim Highland because the oldest exposed crustal rocks in the area are poorly studied. It is beyond doubt, however, that continental crust existed in that lithospheric domain in the Precambrian, most likely as early as Paleoproterozoic. Isotope dating of granites and metamorphic rocks close to central Lake Baikal (west of Vitim) has given mainly Early Paleozoic ages for magmatism and sedimentation (Sm–Nd; 530 ± 23 Ma) as well as for metamorphism and folding (U–Pb zircon; 485 ± 5 Ma) (Fedorovsky, 1997). However, zircon dating of gneisses and migmatites in central parts of metamorphic core complexes yielded mainly Precambrian ages (0.45–2.4 Ga). The relic zircons with ancient ages are interpreted as remnants of a reworked Paleoproterozoic crustal protolith. Kovalenko et al. (2004) found that the Paleozoic granitoids east of Lake Baikal have Precambrian Nd isotope model ages. Taken together, those data strongly suggest the existence of an ancient (Paleoproterozoic or older) crust beneath the Early Paleozoic complexes (Fedorovsky, 1997). This situation is typical of other magmatic and metamorphic complexes within the Caledonian orogenic system in the Baikal region, as argued earlier by Kovalenko et al. (1990), as well as in many orogens worldwide (Rino et al., 2004).

In general, our results on the xenoliths indicate the formation of the Vitim CLM by partial melting at roughly the same time as the formation of oldest known crustal rocks in the region, implying a long-term mantle–crust coupling. Later on, the Caledonian orogeny was followed by widespread formation of granites ($\geq 80\%$ of exposed basement rocks in the region; Fig. 1). Our xenolith data show no evidence that these events resulted in strong erosion and removal of ancient CLM (at least at depths ≤ 80 km). Moreover, these Paleozoic–early Mesozoic crustal events were not accompanied by

significant disturbances of Sr–Nd–Hf–Os isotope systematics of mantle peridotites sampled by Miocene volcanism (Ionov et al., *in press*; Pearson et al., 2004). Hence, the Vitim CLM has been robust and resistant to tectonic and thermal effects of the crustal events, in spite of its fertile composition. It follows that fertile CLM may be fairly stable in major tectono-thermal events, and that a combination of special conditions may be required for delamination of the lower lithosphere (Gao et al., 2002). One has to note, however, that the Vitim area appears to represent central part of a Precambrian domain. The lithospheric mantle at tectonically active margins of such domains (e.g., near early Caledonian ophiolites or the collision zone with the Siberian craton on the western shore of Lake Baikal; Fig. 1) is much more likely to have been strongly modified and may include mantle sections of accreted island arc and other younger terrains. Unfortunately, mantle xenoliths are not as yet known from such areas in southern Siberia to the best of our knowledge.

The Vitim area did not experience major magmatic or tectonic events between the end of the granitoid magmatism in the Triassic and the onset of basaltic volcanism in the Miocene. Formation of the Baikal rift system took place mainly after the eruption of picritic magma in the Miocene, which brought up to the surface the xenoliths from this study (Delvaux et al., 1997; Ionov, 2002; Logatchev and Zorin, 1987). Moreover, as discussed above, the Vitim area is located beyond the tectonically active part of the BRZ and did not undergo appreciable extension either in the Miocene or after that time. Hence, there are no reasons to consider the Vitim xenolith suite as representative of lithospheric mantle in “young extensional intraplate terrains” (Griffin et al., 1999) either in terms of its age or tectonic setting.

7.6. The provenance of fertile off-craton lithospheric mantle

There is little unequivocal evidence to constrain the tectonic setting during the formation of the Vitim CLM. One can probably rule out direct accretion of convecting asthenosphere to the bottom of the early lithosphere due to conductive cooling alone (without partial melting). The range of major-element com-

position in the Vitim peridotite suite appears to be too broad and too consistent with melt extraction trends to be explained by intrinsic heterogeneity of the convecting upper mantle alone. However, it is not clear whether the partial melting was due to upwelling of convecting upper mantle or, alternatively, it took place in the head of a deep mantle plume. Ionov et al. (1994) and Staudacher and Allegre (1991) showed that isotope compositions of O and He in the Vitim peridotites are similar to those inferred for MORB sources. However, He isotope composition may have been modified by radiogenic isotope decay and fluid percolation in the last 2 Ga (Gautheron and Moreira, 2002). Lower mantle with only minor amounts of subducted components may not have significant differences in O isotope composition with the convecting upper mantle.

It is well known that the ancient (mainly Archean) cratonic mantle is much more refractory than the off-craton (Proterozoic or younger) CLM (Boyd, 1989; Pearson et al., 2003 and references therein). Recently, Griffin et al. (1999) suggested that the Phanerozoic CLM is distinctly more fertile than Proterozoic CLM. Furthermore, Griffin et al. (1999, 2003) used the Vitim xenolith suite as an example of particularly fertile mantle from a young extensional terrain and postulated that it represents recently accreted asthenospheric mantle. As discussed above, the median composition of the Vitim xenoliths is much less fertile than claimed by Griffin et al. (1999, 2003), and there is no evidence for current or recent extensional regime in the Vitim area. Most importantly, the Sr–Nd–Hf–Os isotope data from this study and other work (Ionov et al., *in press*; Pearson et al., 2004) clearly establish a Paleoproterozoic depletion age for the Vitim lithospheric mantle. By contrast, a Phanerozoic age attributed to the Vitim CLM by Griffin et al. (1999, 2003) is not based on any specific xenolith or other evidence.

The ancient isotope age estimates for the Vitim xenoliths, as well as recent Re–Os data on other peridotite suites in the Central Asian Orogenic Belt (CAOB; Ionov et al., 2004), show that the claimed post-Archean compositional evolution of the off-craton CLM is not valid for the mantle beneath the CAOB. Similarly, Rudnick et al. (2004) found no compositional distinction between Proterozoic (~1.9

Ga) and Phanerozoic CLM xenoliths from Hanguoba and Qixia in nearby northern China. We further note that a Phanerozoic age was attributed to the mantle beneath Vitim by Griffin et al. (1999, 2003) contrary to radiogenic isotope data on xenoliths available at the time (Ionov and Jagoutz, 1988; Kovalenko et al., 1990; Pearson et al., 1998). On the other hand, they attributed a Proterozoic age to a CLM domain beneath a Phanerozoic fold belt in south-eastern Australia based on Re–Os data on refractory xenoliths (Handler et al., 1997). Altogether, the xenolith data indicate that bulk mantle compositions cannot be used to infer CLM formation ages. It is possible that the proportion of highly refractory melt residues in the lithospheric mantle has generally decreased from the Archean to the present because of progressive cooling of the Earth's interior (Griffin et al., 1998). However, that general notion cannot be applied to individual peridotite suites to even roughly assess their formation ages based on average modal or chemical composition or vice versa.

8. Summary

- (1) The garnet and spinel facies (~40–80 km) CLM beneath the Vitim highland in southern Siberia is generally fertile in terms of modal and major element compositions. It had not been significantly affected by modal or cryptic metasomatism before a Miocene volcanic eruption brought up xenoliths from this study to surface. The uppermost CLM in the area is distinct in terms of modal, chemical and isotope compositions from the refractory mantle underneath the nearby Siberian craton. The Miocene Vitim suite is also more fertile and less metasomatised than the majority of xenolith suites in alkali basaltic rocks worldwide (Pearson et al., 2003).
- (2) The Vitim lithospheric mantle was created by moderate degrees of melt extraction from a fertile protolith, which may have been similar in composition to the primitive mantle. Estimates of depletion ages obtained from Sm–Nd and Rb–Sr systems in this study are consistent with Re–Os (Pearson et al., 2004) and Hf isotope (Ionov et al., in press) data. Collectively, they indicate Paleoproterozoic (~2 Ga) ages for the depletion events.
- (3) The formation ages of the Vitim CLM and of the oldest known crustal rocks east of Lake Baikal are roughly similar indicating possible long-term crust–mantle coupling. Xenolith data provide no evidence that Caledonian orogeny and voluminous granitoid magmatism in the Paleozoic–Early Mesozoic were accompanied by complete or partial removal of the CLM or by widespread metasomatism in the uppermost mantle (~40–80 km).
- (4) The Vitim CLM was not significantly affected by rifting, extension or thermal erosion at the time of the Miocene volcanic eruption. Hence, the fertile modal and major element compositions and poor development of metasomatism in the peridotite suite from the Miocene tuff are not related to upwelling and accretion of young asthenospheric material in the Cenozoic. Rather, they are due to low degrees of the initial partial melting in the Proterozoic and effective isolation during later lithospheric evolution.

Acknowledgements

DAI is grateful for the assistance to H. Stosch with mineral separation, N. Groschopf, A. Friedrichsen and A. Gurenko with XRF and EPMA analyses, D. Jacob with Sr–Nd isotope work, K.-P. Jochum, B. Stoll and K. Herwig with LA-ICPMS analyses, J.-L. Bodinier and S. Portales with solution ICPMS analyses, and to A.W. Hofmann for support in Mainz. Reviews by Y. Xu and an anonymous reviewer and editorial advice of R. Rudnick are highly appreciated. This research was supported by funding to DAI from Alexander von Humboldt-Stiftung and Max-Planck-Institut für Chemie, to IA from Russian Academy of Sciences, to EJ from the DFG. [RR]

References

- Ashchepkov, I.V., 1991. Deep-seated xenoliths of the Baikal Rift. Nauka, Novosibirsk (in Russian, 160 pp.).
- Ashchepkov, I.V., Dobretsov, N.L., Kalmanovich, M.A., 1989. Garnet peridotite xenoliths from alkalic picritoid and basanitoid of the Vitim Plateau. Trans. (Dokl.) USSR Acad. Sci., Earth Sci. Sect. 302, 156–159.

- Ashchepkov, I.V., Litasov, Y.D., Litasov, K.D., 1996. Garnet peridotite xenoliths from melanephelinites of the Hentei Ridge (southern Trans-Baikal region): evidence for a rising mantle diapir. *Russ. Geol. Geophys.* 37, 121–137.
- Boyd, F.R., 1989. Compositional distinction between oceanic and cratonic lithosphere. *Earth Planet. Sci. Lett.* 96, 15–26.
- Boyd, F.R., Pokhilenko, N.P., Pearson, D.G., Mertzman, S.A., Sobolev, N.V., Finger, L.W., 1997. Composition of the Siberian cratonic mantle: evidence from Udachnaya peridotite xenoliths. *Contrib. Mineral. Petrol.* 128, 228–246.
- Brey, G.P., Köhler, T., 1990. Geothermobarometry in four-phase lherzolites: II. New thermo-barometers, and practical assessment of existing thermobarometers. *J. Petrol.* 31, 1353–1378.
- Delvaux, D., Moeys, R., Stapel, G., Melnikov, A., Ermikov, V., 1995. Paleostress reconstructions and geodynamics of the Baikal region, Central Asia. Part I: palaeozoic and Mesozoic pre-rift evolution. *Tectonophysics* 252, 61–101.
- Delvaux, D., Moeys, R., Stapel, G., Petit, C., Levi, K., Miroshnichenko, A., et al., 1997. Paleostress reconstructions and geodynamics of the Baikal region, Central Asia. Part 2: Cenozoic rifting. *Tectonophysics* 282, 1–38.
- Downes, H., 2001. Formation and modification of the shallow sub-continental lithospheric mantle: a review of geochemical evidence from ultramafic xenolith suites and tectonically emplaced ultramafic massifs of western and central Europe. *J. Petrol.* 42, 233–250.
- Eggins, S.M., Rudnick, R.L., McDonough, W.F., 1998. The composition of peridotites and their minerals: a laser ablation ICP-MS study. *Earth Planet. Sci. Lett.* 154, 53–71.
- Esin, S.V., Ashchepkov, I.V., Ponomarchuk, V.A., 1995. Petrogenesis of alkaline basalts from the Vitim Plateau (Baikal Rift Zone). *UIGGM SB RAS Press, Novosibirsk* (58 pp., in Russian).
- Fedorovskiy, V.S., 1997. Dome tectonics in the Caledonian collision system of western Cisbaikalia. *Geotectonics* 31, 483–497.
- Frey, F.A., Green, D.H., 1974. The mineralogy, geochemistry and origin of lherzolite inclusions in Victorian basanites. *Geochim. Cosmochim. Acta* 38, 1023–1059.
- Gao, S., Rudnick, R.L., Carlson, R.W., McDonough, W.F., Liu, Y.-S., 2002. Re–Os evidence for replacement of ancient mantle lithosphere beneath the North China craton. *Earth Planet. Sci. Lett.* 198, 307–322.
- Garrido, C.J., Bodinier, J.-L., Alard, O., 2000. Incompatible trace element partitioning and residence in anhydrous spinel peridotites and websterites from the Ronda orogenic peridotite. *Earth Planet. Sci. Lett.* 181, 341–358.
- Gautheron, C., Moreira, M., 2002. Helium signature of the subcontinental lithospheric mantle. *Earth Planet. Sci. Lett.* 199, 39–47.
- Glaser, S.M., Foley, S.F., Günther, D., 1999. Trace element compositions of minerals in garnet and spinel peridotite xenoliths from the Vitim volcanic field, Transbaikalia, eastern Siberia. *Lithos* 48, 263–285.
- Griffin, W.L., O'Reilly, S.Y., Ryan, C.G., Gaul, O., Ionov, D.A., 1998. Secular variation in the composition of subcontinental lithospheric mantle: geophysical and geodynamic implications. In: Braun, J., Dooley, J.C., Goleby, B.R., Van Der Hilst, R.D., Klootwijk, C.T. (Eds.), *Structure and evolution of the Australian continent*, Amer. Geophys. Union, Geodynamics Series, vol. 26. American Geophysical Union, Washington, DC, pp. 1–26.
- Griffin, W.L., O'Reilly, S.Y., Ryan, C.G., 1999. The composition and origin of sub-continental lithospheric mantle. In: Fei, Y., Bertka, C.M., Mysen, B.O. (Eds.), *Mantle petrology: field observations and high-pressure experimentation*, Spec. Publ. - Geochem. Soc., vol. 6. Geochemical Society, Houston, pp. 13–45.
- Griffin, W.L., O'Reilly, S.Y., Abe, N., Aulbach, S., Davies, R.M., Pearson, N.J., et al., 2003. The origin and evolution of Archean lithospheric mantle. *Precambrian Res.* 127, 19–41.
- Handler, M.R., Bennett, V.C., Esat, T.M., 1997. The persistence of off-cratonic lithospheric mantle: Os isotopic systematics of variably metasomatised southeast Australian xenoliths. *Earth Planet. Sci. Lett.* 151, 61–75.
- Hellebrand, E., Snow, J.E., Hoppe, P., Hofmann, A.W., 2002. Garnet-field melting and late-stage refertilization in 'residual' abyssal peridotites from the Central Indian Ridge. *J. Petrol.* 43, 2305–2338.
- Hofmann, A.W., 1988. Chemical differentiation of the Earth: the relationship between mantle, continental crust, and oceanic crust. *Earth Planet. Sci. Lett.* 90, 297–314.
- Hofmann, A.W., 1997. Mantle geochemistry: the message from oceanic volcanism. *Nature* 385, 219–229.
- Ionov, D., 2002. Mantle structure and rifting processes in the Baikal–Mongolia region: geophysical data and evidence from xenoliths in volcanic rocks. *Tectonophysics* 351, 41–60.
- Ionov, D.A., 2004. Chemical variations in peridotite xenoliths from Vitim, Siberia: inferences for REE and Hf behaviour in the garnet facies upper mantle. *J. Petrol.* 45, 343–367.
- Ionov, D.A., Hofmann, A.W., 1995. Nb–Ta-rich mantle amphiboles and micas: implications for subduction-related metasomatic trace element fractionations. *Earth Planet. Sci. Lett.* 131, 341–356.
- Ionov, D.A., Jagoutz, E., 1988. Sr–Nd isotopic compositions in minerals of garnet and spinel peridotite xenoliths from the Vitim Plateau: first data on mantle inclusions from the USSR. *Dokl. Akad. Nauk SSSR* 301, 1195–1198 (in Russian).
- Ionov, D.A., Jaguz, E., 1989. Isotope behavior of strontium and neodymium in minerals of granite- and spinel-containing peridotite xenoliths of the Vitim plateau: first data from the USSR on mantle inclusions. *Trans. (Dokl.) USSR Acad. Sci., Earth Sci. Sect.* 301, 232–236.
- Ionov, D.A., Kramm, U., Stosch, H.-G., 1992a. Evolution of the upper mantle beneath the southern Baikal rift zone: a Sr–Nd isotope study of xenoliths from the Bartoy volcanoes. *Contrib. Mineral. Petrol.* 111, 235–247.
- Ionov, D.A., Savoyant, L., Dupuy, C., 1992b. Application of the ICP-MS technique to trace element analysis of peridotites and their minerals. *Geostand. Newsl.* 16, 311–315.
- Ionov, D.A., Ashchepkov, I.V., Stosch, H.-G., Witt-Eickschen, G., Seck, H.A., 1993. Garnet peridotite xenoliths from the Vitim volcanic field, Baikal region: the nature of the garnet-spinel peridotite transition zone in the continental mantle. *J. Petrol.* 34, 1141–1175.

- Ionov, D.A., Harmon, R.S., France-Lanord, C., Greenwood, P.B., Ashchepkov, I.V., 1994. Oxygen isotope composition of garnet and spinel peridotites in the continental mantle: evidence from the Vitim xenolith suite, southern Siberia. *Geochim. Cosmochim. Acta* 58, 1463–1470.
- Ionov, D.A., O'Reilly, S.Y., Ashchepkov, I.V., 1995. Feldspar-bearing lherzolite xenoliths in alkali basalts from Hamar-Daban, southern Baikal region, Russia. *Contrib. Mineral. Petrol.* 122, 174–190.
- Ionov, D.A., O'Reilly, S.Y., Griffin, W.L., 1997. Volatile-bearing minerals and lithophile trace elements in the upper mantle. *Chem. Geol.* 141, 153–184.
- Ionov, D.A., O'Reilly, S.Y., Griffin, W.L., 1998. A geotherm and lithospheric cross-section for central Mongolia. In: Flower, M.J.F., Chung, S.-L., Lo, C.-H., Lee, T.Y. (Eds.), *Mantle dynamics and plate interactions in East Asia*, Amer. Geophys. Union, *Geodynamics Ser.*, vol. 27, pp. 127–153 (Washington, DC).
- Ionov, D.A., Bodinier, J.-L., Mukasa, S.B., Zanetti, A., 2002a. Mechanisms and sources of mantle metasomatism: major and trace element compositions of peridotite xenoliths from Spitsbergen in the context of numerical modeling. *J. Petrol.* 43, 2219–2259.
- Ionov, D.A., Mukasa, S.B., Bodinier, J.-L., 2002b. Sr–Nd–Pb isotopic compositions of peridotite xenoliths from Spitsbergen: numerical modelling indicates Sr–Nd decoupling in the mantle by melt percolation metasomatism. *J. Petrol.* 43, 2261–2278.
- Ionov, D.A., Lassiter, J.C., Hofmann, A.W., 2004. The age of the lithospheric mantle in the Central Asian Orogenic Belt from Os isotope data on xenoliths. *Geochim. Cosmochim. Acta* 68 (supplement, abstr. A712).
- Ionov, D.A., Blichert-Toft, J., Weis, D., 2005. Hf isotope compositions and HREE variations in off-craton garnet and spinel peridotite xenoliths from central Asia. *Geochim. Cosmochim. Acta* (in press).
- Jagoutz, E., Wänke, H., 1986. Sr and Nd isotopic systematics of Shergotty meteorite. *Geochim. Cosmochim. Acta* 50, 939–953.
- Jochum, K.P., Dingwell, D.B., Rocholl, A., Stoll, B., Hofmann, A.W., et al., 2000. The preparation and preliminary characterisation of eight geological MPI-DING reference glasses for in-situ microanalysis. *Geostand. Newsl.* 24, 87–133.
- Johnson, J.S., Gibson, S.A., Thompson, R.N., Nowell, G.M., 2005. Volcanism in the Vitim Field, Siberia: geochemical evidence for a mantle plume beneath the Baikal rift zone. *J. Petrol.* (in press).
- Kempton, P.D., Hawkesworth, C.J., Lopez-Escobar, L., Pearson, D.G., Ware, A.J., 1999a. Spinel±garnet lherzolite xenoliths from Pali Aike: Part 2. Trace element and isotopic evidence on the evolution of lithospheric mantle beneath southern Patagonia. In: Gurney, J.J., Gurney, J.L., Pascoe, M.D., Richardson, S.H. (Eds.), *Proc. 7th Internatl. Kimberlite Conf.*, RedRoof Design, Cape Town, pp. 415–428.
- Kempton, P.D., Lopez-Escobar, L., Hawkesworth, C.J., Pearson, D.G., Wright, D.W., Ware, A.J., 1999b. Spinel±garnet lherzolite xenoliths from Pali Aike: Part 2. Petrography, mineral chemistry and geothermobarometry. In: Gurney, J.J., Gurney, J.L., Pascoe, M.D., Richardson, S.H. (Eds.), *Proc. 7th Internatl. Kimberlite Conf.*, RedRoof Design, Cape Town, pp. 403–414.
- Kern, H., Burlini, L., Ashchepkov, I.V., 1996. Fabric-related seismic anisotropy in upper-mantle xenoliths: evidence from measurements and calculations. *Phys. Earth Planet. Inter.* 95, 195–209.
- Klemme, S., O'Neill, H.S.C., 2000. The near-solidus transition from garnet lherzolite to spinel lherzolite. *Contrib. Mineral. Petrol.* 138, 237–248.
- Kovalenko, V.I., Yarmolyuk, V.V., Ionov, D.A., Jagoutz, E., Lugmair, G.W., Stosch, H.-G., 1990. Mantle evolution in central Asia and development of tectonic structures of the earth's crust. *Geotectonics* 24, 283–292.
- Kovalenko, V.I., Yarmolyuk, V.V., Kovach, V.P., Kotov, A.B., Kozakov, I.K., Salmikova, E.B., et al., 2004. Isotope provinces, mechanisms of generation and sources of the continental crust in the Central Asian mobile belt: geological and isotopic evidence. *J. Asian Earth Sci.* 23, 605–627.
- Litasov, K.D., Foley, S.F., Litasov, Y.D., 2000. Magmatic modification and metasomatism of the subcontinental mantle beneath the Vitim volcanic field (East Siberia): evidence from trace element data on pyroxenite and peridotite xenoliths from Miocene picrobasalt. *Lithos* 54, 83–114.
- Logatchev, N.A., Zorin, Y.A., 1987. Evidence and causes of the two-stage development of the Baikal rift. *Tectonophysics* 143, 225–234.
- McDonough, W.F., Frey, F.A., 1989. Rare earth elements in upper mantle rocks. In: Lipin, B.R., McKay, G.A. (Eds.), *Geochemistry and mineralogy of rare earth elements*. Mineral. Soc. America, Washington, DC, pp. 99–145.
- McDonough, W.F., Sun, S.-s., 1995. The composition of the Earth. *Chem. Geol.* 120, 223–253.
- McDonough, W.F., Stosch, H.G., Ware, N.G., 1992. Distribution of titanium and the rare earth elements between peridotitic minerals. *Contrib. Mineral. Petrol.* 110, 321–328.
- Nalivkin, D.V. (ed.), 1965. *Geologic map of the USSR, 1: 2500000*. USSR Ministry of Geology, VSEGEI, NIIGA, SNIIGIMS (in Russian).
- Nickel, K.G., 1986. Phase equilibria in the system SiO₂–MgO–Al₂O₃–CaO–Cr₂O₃ (SMACCR) and their bearing on spinel/garnet lherzolite relationships. *Neues Jahrb. Mineral. Abh.* 155, 259–287.
- Nickel, K.G., Green, D.H., 1985. Empirical geothermobarometry for garnet peridotites and implications for the nature of the lithosphere, kimberlites and diamonds. *Earth Planet. Sci. Lett.* 73, 158–170.
- Niu, Y., 1997. Mantle melting and melt extraction processes beneath ocean ridges: evidence from abyssal peridotites. *J. Petrol.* 38, 1047–1074.
- O'Neill, H.S.C., 1981. The transition between spinel lherzolite and garnet lherzolite, and its use as a geobarometer. *Contrib. Mineral. Petrol.* 77, 185–194.
- Palme, H., O'Neill, H.S.C., 2003. Cosmochemical estimates of mantle composition. In: Carlson, R.W. (Ed.), *Treatise on geochemistry, The mantle and core*, vol. 2. Elsevier, pp. 1–38.

- Pearce, N.J.G., Perkins, W.T., Westgate, J.A., Gorton, M.P., Jackson, S.E., Neal, S.R., et al., 1997. A compilation of new and published major and trace element data for NIST SRM 610 and NIST SRM 612 glass reference materials. *Geostand. Newsl.* 21, 115–144.
- Pearson, D.G., 1999. The age of continental roots. *Lithos* 48, 171–194.
- Pearson, D.G., Nowell, G.M., 2002. The continental lithospheric mantle: characteristics and significance as a mantle reservoir. *Philos. Trans. R. Soc. Lond., A* 360, 2383–2410.
- Pearson, D.G., Ionov, D.A., Carlson, R.W., Shirey, S.B., 1998. Lithospheric evolution in circum-cratonic settings: a Re–Os isotope study of peridotite xenoliths from the Vitim region, Siberia. *Mineral. Mag.* 62A, 1147–1148.
- Pearson, D.G., Irvine, G.J., Carlson, R.W., Kopylova, M.G., Ionov, D.A., 2002. The development of lithospheric keels beneath the earliest continents: time constraints using PGE and Re–Os isotope systematics. In: Fowler, C.M.R., Ebinger, C.J., Hawkesworth, C.J. (Eds.), *The early earth: physical, chemical and biological development*, Spec. Publ. - Geol. Soc. Lond., vol. 199, pp. 65–90.
- Pearson, D.G., Canil, D., Shirey, S.B., 2003. Mantle samples included in volcanic rocks: xenoliths and diamonds. In: Carlson, R.W. (Ed.), *Treatise on geochemistry, The mantle and core*, vol. 2. Elsevier, pp. 171–276.
- Pearson, D.G., Irvine, G.J., Ionov, D.A., Boyd, F.R., Dreibus, G.E., 2004. Re–Os isotope systematics and Platinum Group Element fractionation during mantle melt extraction: a study of peridotite xenoliths from N. Lesotho and S. Namibian kimberlites, the Vitim volcanic field and massif peridotites from Beni Bousera. *Chem. Geol.* 208, 29–59.
- Petit, C., Koulakov, I., Deverchère, J., 1998. Velocity structure around the Baikal rift from teleseismic and local earthquake traveltimes and geodynamic implications. *Tectonophysics* 296, 125–144.
- Petit, C., Déverchère, J., Calais, E., San'kov, V., Fairhead, D., 2002. Deep structure and mechanical behavior of the lithosphere in the Hangai-Hövsngöl region, Mongolia: new constraints from gravity modeling. *Earth Planet. Sci. Lett.* 197, 133–149.
- Poudjom Djomani, Y.H., O'Reilly, S.Y., Griffin, W.L., Morgan, P., 2001. The density structure of subcontinental lithosphere through time. *Earth Planet. Sci. Lett.* 184, 605–621.
- Press, S., Witt, G., Seck, H.A., Ionov, D.A., Kovalenko, V.I., 1986. Spinel peridotite xenoliths from the Tariat Depression, Mongolia: I. Major element chemistry and mineralogy of a primitive mantle xenolith suite. *Geochim. Cosmochim. Acta* 50, 2587–2599.
- Rampone, E., Bottazzi, P., Ottolini, L., 1991. Complementary Ti–Zr anomalies in orthopyroxene and clinopyroxene in mantle peridotites. *Nature* 354, 518–520.
- Rasskazov, S.V., 1994. Magmatism related to the Eastern Siberia rift system and the geodynamics. *Bull. Cent. Rech. Explor. Prod. Elf-Aquitaine* 18, 437–452.
- Reisberg, L., Lorand, J.P., 1995. Longevity of sub-continental mantle lithosphere from osmium isotope systematics in orogenic peridotite massifs. *Nature* 376, 159–162.
- Rino, S., Komiya, T., Windley, B.F., Katayama, I., Motoki, A., Hirata, T., 2004. Major episodic increases of continental crustal growth determined from zircon ages of river sands; implications for mantle overturns in the Early Precambrian. *Phys. Earth Planet. Inter.* 146, 369–394.
- Robinson, J.A.C., Wood, B.J., 1998. The depth of the spinel to garnet transition at the peridotite solidus. *Earth Planet. Sci. Lett.* 164, 277–284.
- Rudnick, R.L., Gao, S., Ling, W.-l., Liu, Y.-s., McDonough, W.F., 2004. Petrology and geochemistry of spinel peridotite xenoliths from Hannuoba and Qixia, North China craton. *Lithos* 77, 609–637.
- Salnikova, E.B., Kozakov, I.K., Kotov, A.B., Kröner, A., Todt, W., Bibikova, E.V., et al., 2001. Age of Palaeozoic granites and metamorphism in the Tuvino-Mongolian Massif of the Central Asian Mobile Belt: loss of a Precambrian microcontinent. *Precambrian Res.* 110, 143–164.
- Sherman, S.I., Dem'yanovich, V.M., Lysak, S.V., 2004. Active faults, seismicity and recent fracturing in the lithosphere of the Baikal rift system. *Tectonophysics* 380, 261–272.
- Shirey, S.B., Walker, R.J., 1998. The Re–Os isotope system in cosmochemistry and high-temperature geochemistry. *Annu. Rev. Earth Planet. Sci.* 26, 423–500.
- Staudacher, T., Allegre, C.J., 1991. Cosmogenic neon in ultramafic nodules from Asia and in quartzite from Antarctica. *Earth Planet. Sci. Lett.* 106, 87–102.
- Stern, C.R., Saul, S., Skewes, M.A., Futa, K., 1986. Garnet peridotite xenoliths from the Pali-Aike alkali basalts of southernmost South America. In: Ross, J. (Ed.), *4th Int. Kimb. Conf., Perth, Kimberlites and Related Rocks*, vol. 2. Spec. Publ. - Geol. Soc. Aust., vol. 14, pp. 735–744.
- Stosch, H.-G., Lugmair, G.W., Kovalenko, V.I., 1986. Spinel peridotite xenoliths from the Tariat Depression, Mongolia: I. Geochemistry and Nd and Sr isotopic composition and their implications for the evolution of the subcontinental lithosphere. *Geochim. Cosmochim. Acta* 50, 2601–2614.
- Sun, S.S., McDonough, W.F., 1989. Chemical and isotopic systematics of oceanic basalts: implications for mantle composition and processes. In: Saunders, A.D., Norry, M.J. (Eds.), *Magmatism in the ocean basins*, Spec. Publ. - Geol. Soc. Lond., vol. 42, pp. 313–345.
- Takazawa, E., Frey, F.A., Shimizu, N., Obata, M., 2000. Whole rock compositional variations in an upper mantle peridotite (Horoman, Hokkaido, Japan): are they consistent with a partial melting process. *Geochim. Cosmochim. Acta* 64, 695–716.
- Van Orman, J.A., Grove, T.L., Shimizu, N., 2001. Rare earth element diffusion in diopside: influence of temperature, pressure, and ionic radius, and an elastic model for diffusion in silicates. *Contrib. Mineral. Petrol.* 141, 687–703.
- Van Orman, J.A., Grove, T.L., Shimizu, N., Layne, G.D., 2002. Rare earth element diffusion in a natural pyrope single crystal at 2.8 GPa. *Contrib. Mineral. Petrol.* 142, 416–424.
- Walter, M.J., 2003. Melt extraction and compositional variability in mantle lithosphere. In: Carlson, R.W. (Ed.), *Treatise on geochemistry, The mantle and core*, vol. 2. Elsevier, pp. 363–394.

- Webb, S.A.C., Wood, B.J., 1986. Spinel–pyroxene–garnet relationships and their dependence on Cr/Al ratio. *Contrib. Mineral. Petrol.* 92, 471–480.
- Wiechert, U., Ionov, D.A., Wedepohl, K.H., 1997. Spinel peridotite xenoliths from the Atsagin-Dush volcano, Dariganga lava plateau, Mongolia: a record of partial melting and cryptic metasomatism in the upper mantle. *Contrib. Mineral. Petrol.* 126, 345–364.
- Xu, X., O'Reilly, S.Y., Griffin, W.L., Zhou, X., 2000. Genesis of young lithospheric mantle in southeastern China: an LAM-ICPMS trace element study. *J. Petrol.* 41, 111–148.
- Zindler, A., Hart, S., 1986. Chemical geodynamics. *Annu. Rev. Earth Planet. Sci.* 14, 493–571.
- Zindler, A., Jagoutz, E., 1986. Mantle cryptology. *Geochim. Cosmochim. Acta* 52, 319–333.